MECHANISTIC STUDIES OF THE THERMAL SPIROPYRAN-MEROCYANINE INTERCONVERSION USING KINETIC ANALYSIS, ION MOBILITY-MASS SPECTROMETRY AND QUANTUM CHEMICAL COMPUTATION METHODS

by

Robert Aaron Rogers, B.S.

A thesis submitted to the Graduate Council of
Texas State University in partial fulfillment
of the requirements for the degree of
Master of Science
with a Major in Chemistry
August 2014

Committee Members:

William J. Brittain, Chair

Todd W. Hudnall

Alexander Kornienko

FAIR USE AND AUTHOR'S PERMISSION STATEMENT

Fair Use

Duplicate Permission

ACKNOWLEDGEMENTS

The author would like to acknowledge all three committee members responsible for supervision and guidance of this work; Dr. W. J. Brittain, Dr. T. W. Hudnall and Dr. A. Kornienko. Many thanks go to Dr. X. Li for his generous support in ion mobility-mass spectrometry studies and Dr. C. Dorsey for his support and training in computational methods and protocols. Without their help, none of this would have been possible.

In addition to the aforementioned people, the author would also like to acknowledge the essential contributions of fellow students Allison Rodier, Jake Stanley, Nick Douglas and Katherine Martin for their assistance in synthesis of the compounds studied herein and their contributions to the experimental and theoretical approaches presented.

Other faculty members whose help was invaluable are Dr. D. Easter and Dr. M. Chung for their helpful discussions of kinetic analysis and Matlab code development for data processing, respectively.

TABLE OF CONTENTS

LIST OF TABLES

Table **Page**

LIST OF FIGURES

Figure **Page**

ABSTRACT

The spiropyran-merocyanine system of four derivatives of the parent spiropyran system were studied on the thermal merocyanine to spiropyran interconversion pathway using kinetic analysis, ion mobility-mass spectrometry and several supplemental computational approaches. The effect of tethering a spiropyran moiety to the surface of a silica nanoparticle suspended in ethanol was kinetically characterized. Ion mobility mass-spectrometry chromatographs of three derivatives were analyzed for conformers of spiropyran detected in the gas phase. Three singly charged monomeric conformer groups were identified for all derivatives used in ion mobility-mass spectrometry studies and were assigned to the spiropyran, *cisoid* and *transoid* isomers based on theoretical collision cross-sections of potential isomers. Collision cross-sections were predicted through optimization of seven protonated spiropyran isomers at the DFT-B3LYP/6-31G++(d,p) level of theory followed by analysis using the program MOBCAL. Six spiropyran isomers for three of the most photoactive spiropyrans studied were identified to be the dominant isomers on the thermal MC to SP interconversion pathway and their geometries were optimized at the DFT-B3LYP/6-31G++(d',p') level of theory with the inclusion of the conductor-like polarizable continuum model for methanol solvent (CPCM). Following geometric optimization, ZINDO/CPCM and TDDFT-B3LYP/CPCM were used to predict the absorption maxima of each geometric isomer and isomer-specific rate constants were determined through conventional UV-visible spectroscopic analysis. Based on the collective results of each portion of this work, phase-dependent mechanisms for the thermal MC to SP interconversion are postulated.

I. INTRODUCTION

Spiropyrans are a special derivative of pyrans first discovered in the 1950's.[1,2] Spiropyrans exhibit unique behavior when stimulated with electromagnetic radiation, primarily in the ultraviolet (UV) or visible ranges of the spectrum. Observed by the naked eye as a significant color change in solution phase experiments, spiropyrans undergo a geometric reconfiguration called "photochromism." Upon exposure to UV light, the geometry of each molecule is transformed from an orthogonal orientation of two planar ring systems (the indole and phenolate moieties) connected at a chiral, "spirocarbon" center to a coplanar, prochiral configuration of the two ring systems accompanied by a change in the bonding character of the spirocarbon.

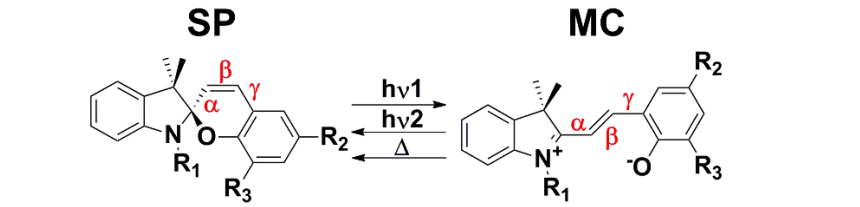

SP1: R_1 = Me, R_2 = NO_2, R_3 = H
SP2: R_1 = Me, R_2 = NO_2, R_3 = OMe
SP3: R_1 = Me, R_2 = Cl, R_3 = H
SP4: R_1 = $(CH_2)_4CCH$, R_2 = NO_2, R_3 = H

Scheme 1 The general reaction of spiropyran. ($h\nu_1$), ($h\nu_2$), and (Δ) denote UV, visible and thermal processes, respectively. MC isomer nomenclature follows the configuration of the three bridging bonds (α, β and γ) with either a *cis* (C) or *trans* (T) designation.

The basic structure of the ring-closed spiropyran (SP) and the ring-opened merocyanine (MC), along with the derivatives examined herein, are shown in Scheme 1. The primary features of interest for these systems are the bonding character of the spirocarbon of the pyran ring and the ethylene bridge geometry with bonds denoted (α), (β) and (γ) as well as the spirocarbon-oxygen bond of the central pyran ring. When the colorless SP form of spiropyran is exposed to UV radiation ($h\nu_1$), the spirocarbon-oxygen bond of the pyran ring is

cleaved, resulting in the formation of a *cisoid*-MC intermediate followed by *cis*→*trans* isomerization to the *transoid*-MC isomers, exhibiting the evolution of color and the formation of an extended π-conjugated electronic configuration. From the MC state, either visible irradiation ($h\nu_2$) or heat (Δ) will induce the reformation of the spirocarbon-oxygen bond of the pyran ring and the system will revert back to a colorless SP state. Nomenclature for the MC isomers follows the αβγ configuration of the ethylene bridge. An MC isomer with a configuration like that shown in Scheme 1 would be called the TTC isomer. The MC isomers may also be further divided into two categories; the *cisoid*-MC (XCX) and *transoid*-MC (XTX) isomers, where categorization depends on the configuration of the (β) bond. All eight MC isomers are shown in Scheme 2 divided into their respective *cisoid* and *transoid* categories. Note that the presence of (X) in isomer group designations refers to both the *cis* and *trans* bond configurations collectively.

SP1-4 were chosen for several reasons depending on the section of this work in which they were used. Each derivative represents a contrast with the others in various aspects of kinetic reactivity and electronic characteristics. **SP1** was chosen due to its widespread use within the literature and its commercial availability. **SP2** was chosen because its equilibrium concentrations between spiropyran and merocyanine geometries is significantly different from **SP1**,**3-4**. **SP3** is unique in that it is generally unreactive, even under intense irradiation conditions and finally **SP4** was chosen because the hexyne moiety substituted at the indole nitrogen allows its use in "click" chemistry for chemical modification of silica nanoparticles. **SP4** also provides insight into the difference in reactivity when indole nitrogen substituents vary.

Excited state studies of the spiropyran system using transient absorption spectroscopy suggest that for spiropyrans with a nitro substituent located on the phenolate moiety, triplet

excitation plays a major role in the photochemical bond cleavage of the spirocarbon-oxygen bond leading to intersystem crossing from the triplet state to the singlet state followed by relaxation to the ground state MC isomers.[3] Estimates of the internal molecular temperature of the singlet state after internal conversion suggest that the available energy in the singlet state is sufficient to facilitate the formation of a distribution of XTX isomers.[4]

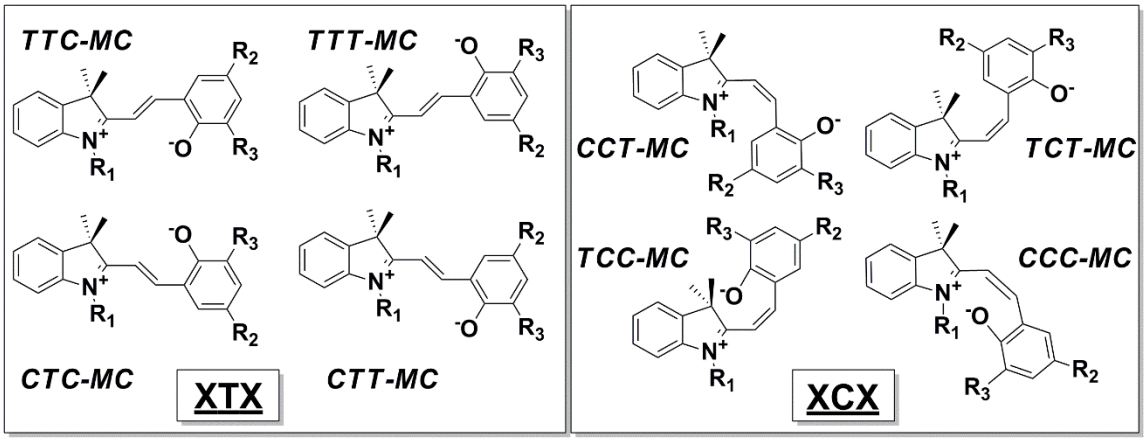

Scheme 2 Structural MC isomers and their respective *cisoid* (XCX) and *transoid* (XTX) categories. Nomenclature of the isomers follows that noted in Scheme 1.

Spiropyran is a heavily studied molecule and has a wide range of applications. A search on Scifinder Scholar® for the term "spiropyran" results in 3627 hits. It is clear that a wealth of information is available pertaining to the mechanism of pyran ring-opening and -closing in spiropyrans yet this complex process on both the thermal and photochemical pathways is still not well understood. Despite the lack of a conclusive, experimentally obtained explanation of its unique properties, there have been many applications of spiropyran that have garnered considerable attention. The most well-known application of spiropyran is in Transitions® Eye Glasses. In outdoor environments the lenses containing spiropyrans change to a dark, UV-blocking lens and when indoors, they change to a clear lens. Other applications of spiropyrans have either been patented or investigated for use in areas such as optical switching and memory

storage,[5–10] colormetric sensing,[11] materials[9,12–19] and light-mediated chromatography.[20–22]

Applications aside, a fundamental understanding of the mechanistic behavior of spiropyran on both the photochemical and thermal pathways is essential for future development of more robust and tunable spiropyran systems. Significant efforts to deduce the mechanism of each pathway have been carried out using theoretical and experimental approaches spawned as a result of attempts to apply spiropyrans in memory and switching applications.[8] Particularly dominant in spiropyran research are spectroscopically based experimental approaches, for obvious reasons, but over the last decade a growing number of investigators have employed a variety of computational techniques and structurally simplified model systems to study the fundamentals of the thermal and photochemical reactions. Though these model systems are often correlated with experimental evidence their structurally simplified nature restricts the universal applicability of the information obtained computationally to the parent system and different conclusions regarding the mechanistic step-by-step processes often result.

In an effort to contribute original research to this ongoing endeavor of understanding the subtle details of such a complex process, several goals are of notable mention. This work can be broken down into three standalone investigations; (1) single-wavelength photochemical reaction kinetics of a spiropyran in solution and surface-bound to a particle, (2) qualitative and semi-quantitative, computationally aided structural stability investigations using ion mobility-mass spectrometry (IM-MS) and (3) quantitative determination of isomer-specific rate constants of the thermal MC to SP interconversion based on qualitative, computationally determined absorption band assignments. Though each project is an independent study with standalone value, the conjunction of the three investigations provides a complete picture of

spiropyran using the latest techniques in theoretical and experimental investigations of photochromic systems on conventional timescales (>1 msec.).

For the single-wavelength kinetics portion of this work, **SP4** in the solution phase was investigated using conventional UV-visible spectroscopy for the thermal MC to SP interconversion. The appropriate first-order reaction of the solvated system was deduced based on three kinetic models at the visible region absorption maximum. In addition to solution phase experiments, kinetics of the thermal MC to SP interconversion were studied for spiropyrans chemically bound to the surface of ~20 ± 3 nm diameter amorphous silica nanoparticles (**SP4**-**NP**) suspended in ethanol. All characterizations for this portion of the work presented exploit the visible region absorption maximum that occurs at around 540 nm in both systems. The kinetic rate constants for the solution and surface bound experiments, using the empirically deduced appropriate kinetic model, were then compared to examine the effects of the microenvironment on the thermal MC to SP interconversion process. The results of the kinetic studies gave rise to the second investigation aimed at addressing the question of which isomers are stable enough to play a role in MC to SP interconversion on the thermal pathway.

The gas-phase structural analysis portion of this work includes several new experimental and computational techniques not previously applied to spiropyrans. **SP1**-**3** were investigated for the first time using IM-MS. Computational modeling of potential conformers in IM-MS experiments was performed by computing the minimum energy configurations of seven protonated spiropyran isomers (CCC, CCT, CTT, CTC, TTT, TTC and SP) at the DFT-B3LYP level of theory using the 6-31G++(d,p) basis set. The computational aspect of the IM-MS investigation differs from previous computational studies by the inclusion of MC and SP

isomer protonation. Inclusion of protonation enabled prediction of the two-dimensional cross-sections (CCS) of all isomers potentially observable in IM-MS chromatographic separations. The isomers studied have been suggested to be the most probable isomers along the photochemical and thermal reaction pathways according to previous computational and experimental assessments.[23–25] Assignment of each conformer group detected in IM-MS experiments was then performed by comparison of the two-dimensional theoretical (CCS) calculations for each isomer to the experimental IM-MS chromatographs.

For the final portion of this work full spectrum kinetic experiments were performed following IM-MS experiments for three of the most photoactive of the four derivatives studied, **SP1** and **SP3**-**4**. Absorption band assignments were carried out using a DFT-B3LYP/ZINDO and DFT-B3LYP/TDDFT approach using the 6-31G++(d',p') basis set with the inclusion of the conductor-like polarizable continuum model (CPCM) for methanol in all isomeric geometry optimizations and absorption spectra predictions. Computational results were then qualitatively compared with experimental spectra to assess the accuracy of the results for each method. Through comparison of the computed absorption maxima, oscillator strengths and relative isomer energies against the experimental photostationary state (PSS) spectra of each derivative, isomer-specific rate constants were determined where non-shifting, and therefore non-convoluted, absorption band maxima occur.

In toto, the three investigations contained herein are discussed collectively to provide a complete picture of the spiropyran system using slow timescale methods (>1 msec.). IM-MS, computational and kinetic results are discussed from an integrated perspective to yield insight into the stepwise progression of the thermal MC to SP interconversion and two separate phase-dependent mechanisms are postulated.

II. EXPERIMENTAL

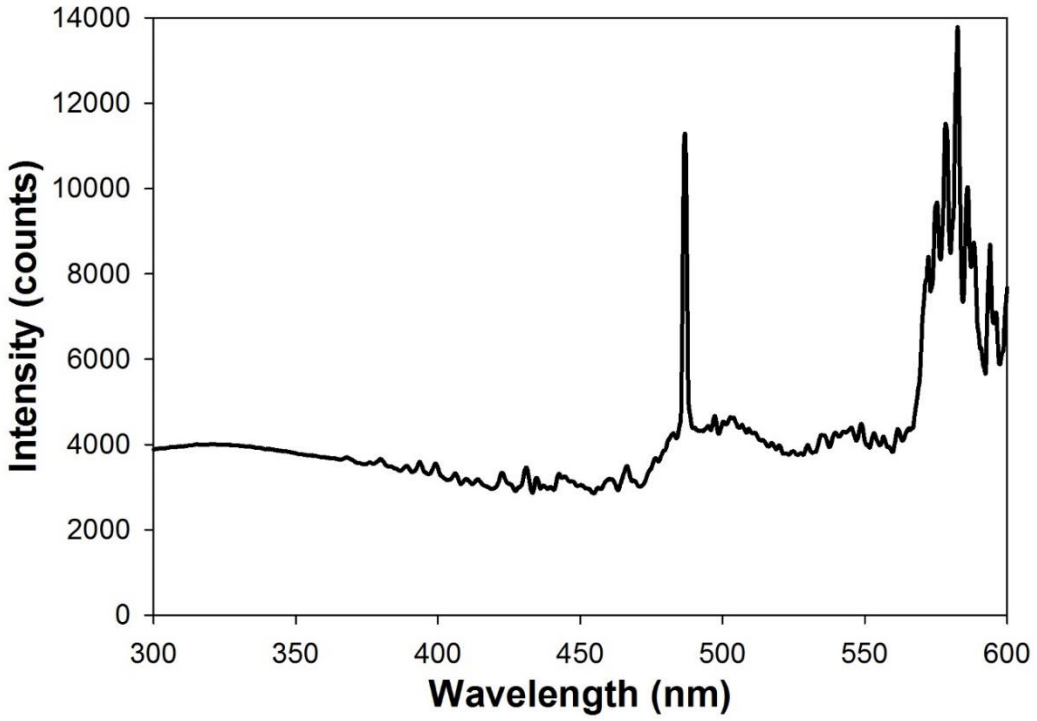

Figure 1 Spectrum of the DH2000 light source

Spectroscopy Instrumentation, Irradiation Instrumentation and Universal Spectral Acquisition Specifications and Instrument Configurations

All spectral and kinetic data acquisitions were performed using an Ocean Optics DH2000 deuterium/halogen light source (spectrum shown in Figure 1), QPOD sample holder with temperature and stir-rate control (~200 rpm) for all trials and an HR2000+ CCD array detector. All components were connected by 600 μm diameter quartz fiber optic cables with SMA905 connectors. All spectra are reported from 300-600 nm wavelengths. The configuration of the detector is as follows; 25 μm slit aperture, no order sorting filter, no

detector collection lens, grating is H1 at 300 nm, integration time of 1 msec., boxcar width of 3, 100 scan averaging, non-linearity correction and electric dark correction enabled. SpectraSuite or OceanView Software (Ocean Optics) was used to acquire the raw data for all spectroscopic measurements. SigmaPlot 12 was used to create all plotted spectra and kinetic regression curves as well as perform least squares fitting routines and error analysis, where appropriate.

Irradiation of all samples was performed using a Newport Power Supply (Part No. 66907) and XeHg Lamp (Part No. 66901) set to a constant power of 160 Watts. Cut-off filters were used (spectra shown in Figure 2) to select either UV (Edmund Optics FSQ-UG11, power at sample = 20.5 fc) or visible (Edmund Optics FSQ-GG400, power at sample = 4.25 kfc) wavelength ranges for irradiation. The irradiation beam was set orthogonally to the probe beam for all spectral acquisitions. The sample volume in all spectroscopic measurements was ~1 mL to optimize exposure of the sample solution to the irradiation and probe beams. A 1 cm quartz cuvette with a septum cap was used for all samples. PSS and equilibrated spectra were recorded by irradiating the sample continuously with either UV or visible light until the absorbance of the visible region peak exhibited no further change with continued irradiation. All thermal kinetic trials were performed by irradiating the sample to the UV PSS and then monitoring the decrease in absorbance of the appropriate maximum wavelength (λ_{max}) in the dark for ≥2 half-lives. The average rate constants were determined using a linear least-squares regression of five trials (solvated vs. nanoparticle section) or four trials (isomer specific rate constant section) using the appropriate first-order kinetic plot. A full statistical analysis of the arithmetic manipulations used on the resultant data was also performed to quantify the experimental error accompanying each reported kinetic parameter.

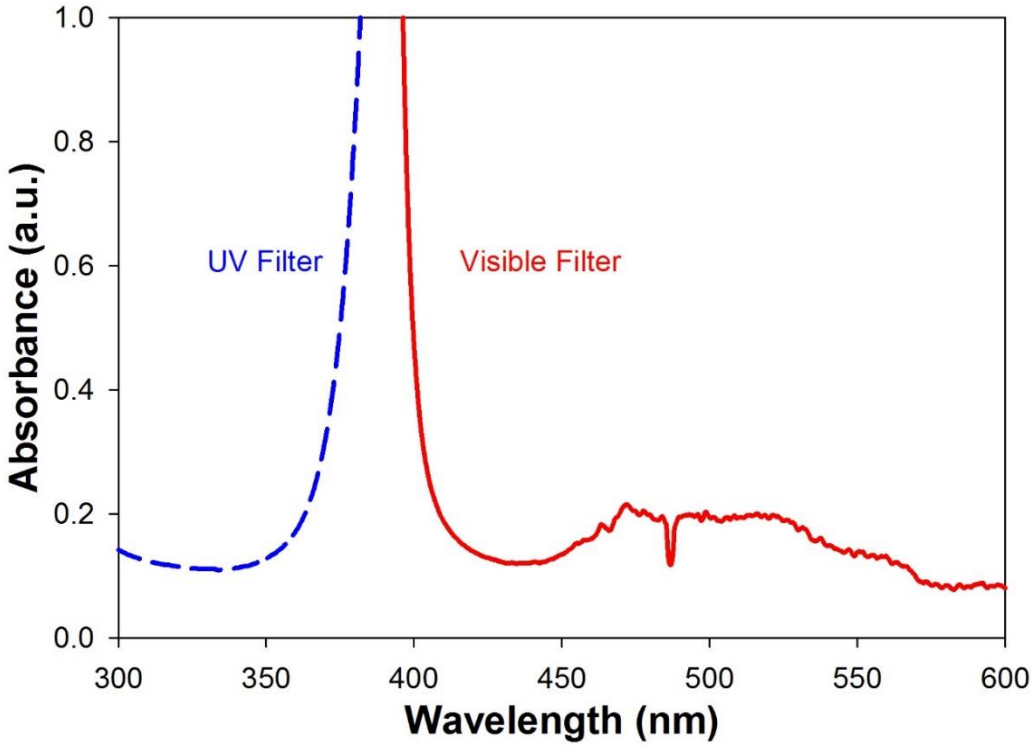

Figure 2 Spectra of the UV and visible irradiation filters used for all experiments

Preparation of **SP1**-**4** and **SP4**-**NP**

SP1 was purchased from Sigma-Aldrich. **SP2**-**4** were generously prepared, according to the literature,[26,27] by other members of our research group, named in the acknowledgements section of this report for their essential contribution to this work.

Thermal Reaction Kinetics of a Spiropyran in Solution and Surface-Bound to a Particle Suspended in Solution

All spiropyran solutions for this portion of the work used ACS spectroscopy grade ethanol (Sigma-Aldrich). Ludox HS-30 amorphous silica nanoparticles (Sigma-Aldrich, diameter = ~20 ± 3 nm) were obtained, dried, ball-milled and then used for chemical modification of the surface of the nanoparticles with **SP4** via "click" chemistry (Scheme 3) to give **SP4**-**NP** modified silica nanoparticles. All solution concentrations are reported as the concentration of **SP4** in the system, whether solvated or chemically bound to silica nanoparticles.

SP4-**NP** solutions were prepared by sonicating an excess of the chemically modified nanoparticles in ethanol for approximately 5 minutes in a volumetric flask with a slightly overfilled amount of solvent. Following sonication, the solution was aerated with N_2 gas for approximately 15 minutes until the liquid level meniscus minima within the volumetric flask reached the fill line and then was tightly capped

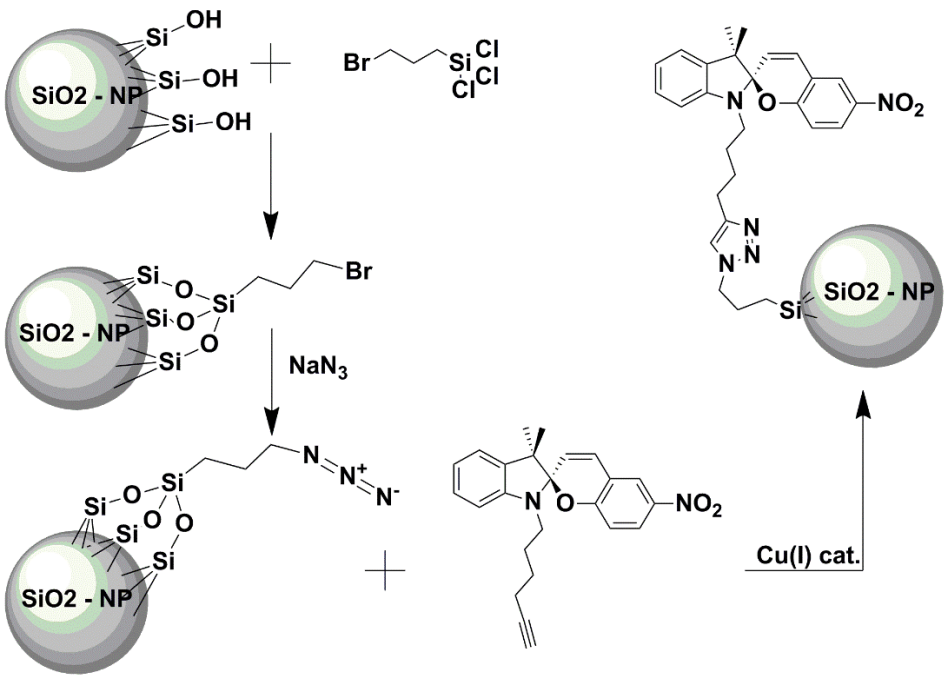

Scheme 3 The "click" reaction for **SP4**-**NP** preparation

and stored for 24 hours in the dark to allow for sedimentation of particle aggregates and equilibration of the **SP4** moieties. After sedimentation was complete, the supernatant solution was decanted and transferred, using air-sensitive techniques, in two equal volumes to identical volumetric flasks. The equilibrated spectra, PSS spectra and kinetic trends were then recorded *ex tempore* for 5 trials using one of the volumetric aliquots. The solvent was removed from the other aliquot and the sedimented nanoparticles were dried and weighed to determine, *ex post*, the concentration of **SP4** according to thermogravimetric analysis of spiropyran surface coverage provided by our synthetic team.

SP4 solutions were prepared gravimetrically using recrystallized compound. A stock solution was prepared and diluted as necessary until an absorbance value of approximately 1 at the UV PSS was obtained. After the target concentration was achieved, the volumetric solutions were filled just past the fill line and aerated with N_2 gas for approximately 15 minutes

until the liquid level meniscus minima reached the fill line of the volumetric flask. The solution was then tightly capped and stored for 24 hours in the dark to equilibrate prior to spectral and kinetic data acquisition.

One preliminary kinetic trial was performed in which the thermal decay of the visible region peak maxima was monitored for 5000 seconds from the UV PSS and plotted using three different kinetic models then compared for accuracy. It should be noted that this preliminary trial was compared with shorter time-length trials to ensure its accuracy. The effect of incorrect measurement of the equilibrated absorption (A_{inf}) at the maximum wavelength being monitored were also investigated to demonstrate the sensitivity of kinetic data to small, experimentally introduced perturbations in equilibrium absorbance. For the thermal kinetic data acquisition, decay of the visible region absorption maxima was recorded every ~3 seconds for 2000 seconds from the UV PSS at a temperature of 23 ^{o}C.

IM-MS Investigations of **SP1-3**

All ion mobility data was obtained using a Waters SYNAPT G2 equipped with a traveling-wave ion mobility separator (TWIMS) in positive ion mode. MassLynx and Driftscope software (Waters) were used for instrument operation and data acquisition. The ion mobility chamber N_2 gas flow was set to 120 mL min^{-1} and the He gas flow was set to 10 mL min^{-1}. Wave velocity and height were set to 750 m sec^{-1} and 35 V, respectively. The source gas flow was set to 0.0 mL min^{-1} and the trap gas flow was set to 0.4 mL min^{-1}. Integration of the ion mobility data over a 30 second period was performed for each drift time measurement. The electrospray ionization (ESI) sample injection pump rate was set to 6.00 μL min^{-1}.

All samples of **SP1**-**3** were recrystallized prior to use. Each sample was then dissolved in methanol to a concentration of ~0.5 mg mL^{-1} and equilibrated for ~24 hours in the dark prior to use. Following equilibration, each solution was volumetrically diluted by a factor of 50. The total volume per sample of each solution used in equilibrated drift time measurements was ~1 mL in a quartz cuvette. 50 μL of each equilibrated solution was then placed into a 100 μL syringe for injection into the ESI source. All samples were prepared at room temperature.

Methanol solutions of **SP1**-**3** were irradiated in the same quartz cuvette as the equilibrated samples and were transferred following irradiation, *ex tempore*, into the ESI source. All irradiations were performed using either a Dolan Jenner DC-950 or MH-100 light source. Band selection was performed by filtering the light source output with colored glass filters from Edmund Optics (Models UG-11 or GG-400; spectra in Figure 2). Irradiation times were ~3 minutes with stirring at room temperature. This amount of time has been determined to be sufficient for reaching a PSS within all systems studied using the irradiation equipment noted above.

Sheng, et. al.[23] identified ground, singlet and triplet state geometries for a model spiropyran. In order to accurately assess the ground state structures of the three spiropyran derivatives used in this study, the Cartesian coordinates provided by Sheng, et. al. for the ground state conformations of the MC isomers were used as base structures from which we modified and optimized the geometries of our derivatives according to the DFT-B3LYP method using the 6-31++G(d,p) basis set.[28–31] All structures were calculated in the protonated form to accurately reflect the product of electrospray ionization, where the proton reportedly binds to the indole nitrogen or the phenolate oxygen for the SP and MC isomers, respectively.[32,33] It should be noted that the TCT isomer and TCC isomers are greatly

unfavored when the dimethyl substitution of the indole pentane ring is included in the structure, as noted in the literature.[23] In fact, upon optimization, the TCC isomer reverts to a geometry better described as the CCT. For this reason, only the SP, CCT, CCC, and all XTX MC isomers were considered. All geometry optimizations were performed using the Gaussian 09 software package.[34]

Theoretical CCS values were calculated with the MOBCAL program developed by Martin Jarrold's group at Indiana University—Bloomington, available for free online.[35,36] Cartesian coordinates from DFT-B3LYP isomeric geometry optimizations were imported directly into the program for each structure. Only the projection approximation method (PA) and trajectory method (TJ) results are reported for these small molecule systems.

OriginPro 8.5 was used to evaluate plots of drift time (t_d) vs. percent relative intensity using the peak finding function incorporated into the program based on a Gaussian distribution about the peak center. Chromatographic data was normalized to a percent relative intensity of 100% for the largest peak in each spectrum. Following normalization, the resulting area under each peak after deconvolution (example in Figure 3) was determined by the software from which a total area could be obtained. The fraction of the total area represented by each peak can be considered approximately equal to the mole fraction of each isomer in the sample assuming that all isomers have similar ionization efficiency. The residuals of each fit were also calculated.

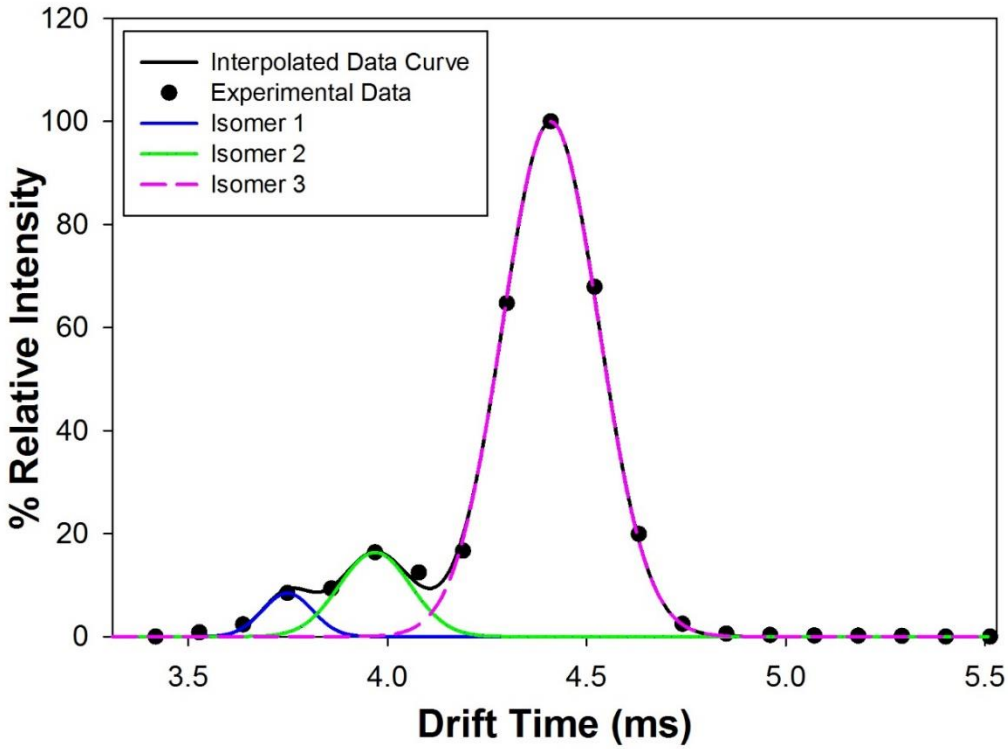

Figure 3 Deconvolution example for IM-MS chromatographs assuming Gaussian peak shape

Isomer-Specific Rate Constants of the Thermal MC to SP Interconversion and Computationally Determined Absorption Band Assignments for **SP1**, **SP2** and **SP4**

Similar to the optimization performed for the IM-MS portion of this work, the geometries of the same seven isomers provided by Sheng and co-workers were modified to reflect the full structure of the derivatives and reoptimized using the DFT-B3LYP method with the 6-31G++(d',p') basis set.[28–31] For this first step, the optimization was performed with the inclusion of the conductor-like polarizable continuum model (CPCM)[37,38] for methanol to specify more appropriate conditional constraints on the system. It should be noted that in all cases, the CCT isomer assumed the ring-closed SP geometry and so all further calculations

included only the six SP, CCC and XTX isomers. Also, frequency checks performed for **SP4** following optimization resulted in single imaginary frequencies for the SP, CTC, CTT and TTT isomers. These were ignored after repeated attempts to eliminate them using tighter convergence criteria. The noted imaginary frequencies seem to be a result of the hexyne moiety bending out of plane with the indole ring system. These isomeric geometries are predicted to be more stable in many previously published computational studies and we feel that their impact on the physical interpretation of each **SP4** isomer in these specific instances is negligible.

Following the initial optimizations, both the ZINDO(closed-shell)/CPCM-Methanol method[37–47] and TDDFT-B3LYP(6-31G++(d'p'))/CPCM-Methanol[37,38,48–54] method were used to calculate theoretical electronic transition energies and oscillator strengths for the energy minimized structures of each derivative. The energies and relative order of stability are reported and the frontier orbitals involved in the high oscillator strength, primary transitions are provided. All geometry optimizations, solvent modelling and excitation spectra calculations were performed using the Gaussian 09 software package.[34]

Kinetic sample solutions of **SP1**, **SP2** and **SP4** were prepared using ACS spectroscopy grade methanol (Sigma-Aldrich) to mimic the conditions of IM-MS experiments up to the point of injection into the ESI source. All sample concentrations were determined gravimetrically. All sample solutions were slightly overfilled in volumetric flasks and sonicated in a bath and then aerated with N_2 gas for ~15 minutes until the liquid level meniscus minima reached the fill line. The solutions were then tightly capped and stored in the dark for ~24 hours prior to use in kinetic and spectral data acquisition. The spectra acquired here were also smoothed using a Savitzky-Golay filter[55–60] (polynomial order = 3, frame size = 201 pixels)

built into Matlab 2013a. An example of Savitzky-Golay filtering applied to experimental spectra is shown in Figure 4. Savitzky-Golay filtering enabled removal of spectral lines from the deuterium/halogen probe source and easier identification of absorption maxima. (R^2) values for each time trial were checked to ensure accurate smoothing ($R^2 \geq 0.995$) for all kinetic data.

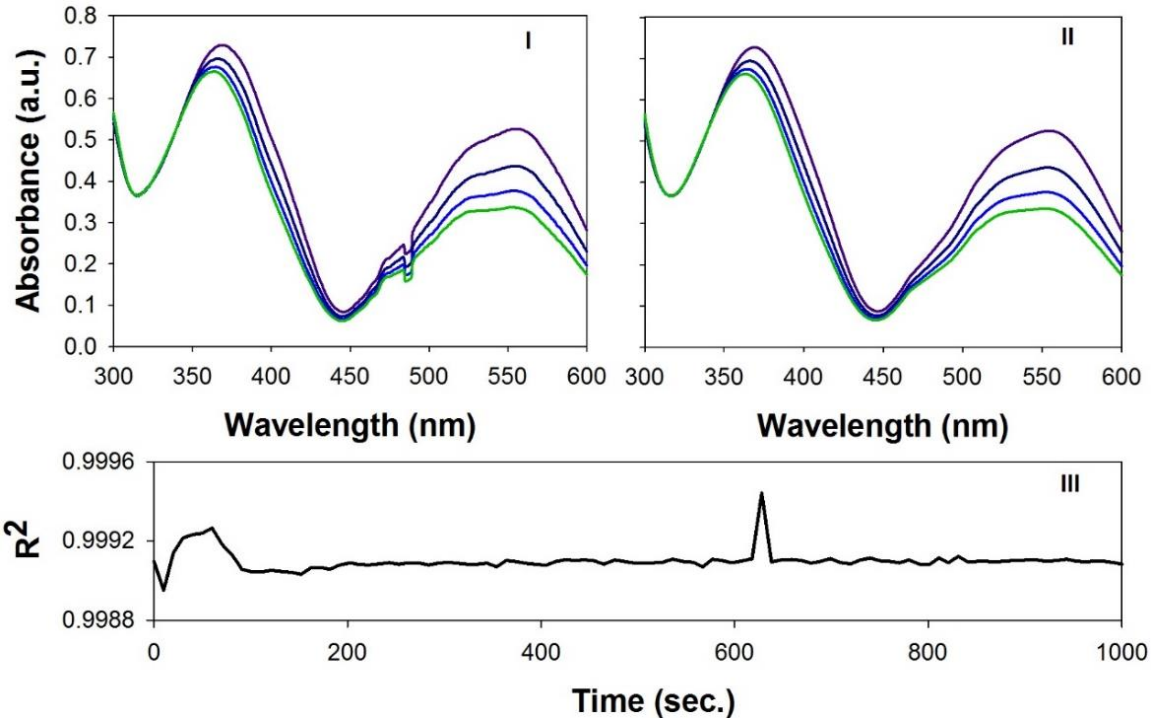

Figure 4 Experimental spectra before (I) and after (II) Savitzky-Golay filtering. (III) shows R^2 values for filtered spectra gathered every 10 seconds for 1000 seconds.

Each kinetic trial was performed four times for each derivative at a temperature of 40 ^{o}C. The full spectrum of each sample solution was recorded every ~10 seconds from the UV PSS until equilibrium was reached, or for ~500 seconds, whichever came first. The equilibrium concentrations of each sample were recorded prior to irradiation to the UV PSS for use as the equilibrium absorbance value in kinetic analysis (A_{inf}). The UV PSS spectra and equilibrium spectra of each compound were then compared with experimental spectra to

qualitatively assign absorption maxima for each spectral prediction method to specific isomers where possible, extract maximum wavelength shifts, and justify the choice of absorption band used for kinetic characterization. The accuracy of each computational spectrum prediction method is discussed. Irradiation experiments with visible light were not performed for this portion of the work because the equilibrium lies almost completely toward the ring-closed SP isomer and irradiation with visible light results in a negligible change in the absorption spectra of each derivative.

III. RESULTS

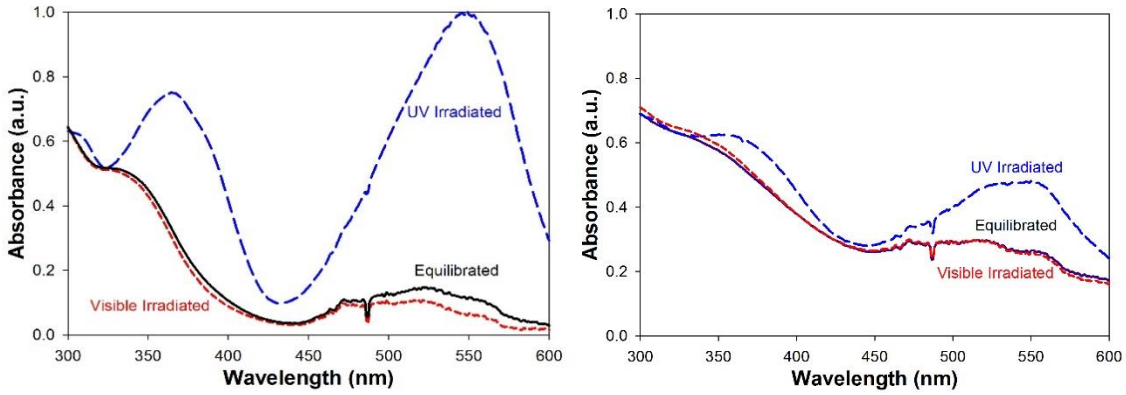

Figure 5 PSS and equilibrated spectra of **SP4** (left) and **SP4-NP** (right) in ethanol

Thermal Reaction Kinetics of a Spiropyran in Solution and Surface-Bound to a Particle Suspended in Solution

The PSS spectra of **SP4** and **SP4**-**NP** are shown in Figure 5, respectively. Irradiation of the **SP4** solution with UV light causes an increase in the visible region peak, attributed to the MC isomers, while irradiation with visible light leads to a decrease in the visible absorption peak. The values of λ_{max} for **SP4**-**NP** and **SP4** are 551 and 548 nm, respectively, indicating a particle induced bathochromic shift of ~3 nm. Also of note is the negligible change in the spectrum of **SP4**-**NP** with visible irradiation. This is counter intuitive due to the more polar nature of the silica nanoparticle surface as compared to the ethanol suspension media.

The spiropyran thermal reaction from MC → SP is typically characterized as a first-order formal kinetic process having a rate law of the form;

$$\frac{d[MC]}{dt} = -k[MC] \qquad \textbf{Equation 1}$$

where, [MC] is the concentration (in M) of the MC isomers and (k) is the first-order rate constant (in s^{-1}). Integration of this model is straight forward and gives the following integrated rate Equation;

$$\ln([MC]_t) = -kt + \ln([MC]_0) \qquad \textbf{Equation 2}$$

where $[MC]_t$ and $[MC]_0$ are the concentrations of the merocyanine isomers at time, (t), and (t = 0), respectively. The concentration of the MC isomers is directly proportional to the absorbance of the visible region peak associated with the MC isomers according to the Beer-Lambert Law;

$$A = \varepsilon bc \qquad \textbf{Equation 3}$$

where (A) is the absorbance (in a.u.) of the solution at λ_{max}, (ε) is the molar extinction coefficient (in a.u. $M^{-1}\,cm^{-1}$) and (c) is the concentration (in M) of the species responsible for absorption at λ_{max}. The absorbance of the visible region peak associated with the MC isomers is then directly proportional to the concentration of MC isomers at any time and the integrated rate law may take the form;

$$\ln(A_t) = -kt + \ln(A_0) \qquad \textbf{Equation 4}$$

Equation 4 represents the formal kinetic rate law that may be used to characterize a simple first-order reaction that proceeds only in one direction and having only a single reactant and a single product.

Another case of first-order behavior that differs from Equation 4 occurs when there is a competing back reaction. For the spiropyran system this can be generalized by the following reaction;

$$MC \underset{k_{-1}}{\overset{k_1}{\rightleftharpoons}} SP \qquad \textbf{Equation 5}$$

where (k_1) and (k_{-1}) are the forward and reverse rate constants of the equilibrium reaction. For this reaction, the general rate law may be given by;

$$-\frac{d[SP]}{dt} = \frac{d[MC]}{dt} = -(k_1)[MC] + (k_{-1})[SP] \qquad \textbf{Equation 6}$$

At equilibrium, the overall rate of change in concentration of each species approaches zero and the following result is obtained in terms of the infinite time concentrations of MC and SP, $[MC]_{inf}$ and $[SP]_{inf}$, which may be equated with their equilibrium concentrations;

$$0 = (k_{-1})[SP]_{inf} - (k_1)[MC]_0 \qquad \textbf{Equation 7}$$

The equilibrium constant (K_{eq}) is then easily obtained by rearrangement of Equation 7 to give;

$$\frac{k_1}{k_{-1}} = \frac{[SP]_{inf}}{[MC]_{inf}} = K_{eq} \qquad \textbf{Equation 8}$$

The concentration of SP at infinite time can be written in terms of the concentrations of MC at (t = *0*) and (t = infinity);

$$[SP]_{inf} = [MC]_0 - [MC]_{inf} \qquad \textbf{Equation 9}$$

Combining Equations 8 and 9 and substituting into Equation 6 gives;

$$\frac{d[MC]}{dt} = -(k_1 + k_{-1})([A]_t - [A]_{inf}) \qquad \textbf{Equation 10}$$

Finally, integration of the derived rate law above results in the integrated rate Equation for an equilibrium first-order equilibrium reaction of MC ⇌ SP;

$$\ln([A]_t - [A]_{inf}) = -(k_{obs})t + \ln([A]_0 - [A]_{inf}) \qquad \textbf{Equation 11}$$

where (k_{obs}) is the observed rate constant and is equal to ($k_1 + k_{-1}$). Equation 11 may be rearranged to the following form, which is sometimes reported in the literature, but is algebraically identical;

$$\ln\left(\frac{[A]_t - [A]_{inf}}{[A]_0 - [A]_{inf}}\right) = -(k_{obs})t \qquad \textbf{Equation 12}$$

The variation in literature resources pertaining to the choice of rate law is significant and as a result, a sample of **SP4** was monitored for 7000 seconds and plotted according to Equations 4, 11 and 12. The results of each of these plots are shown in Figure 6.

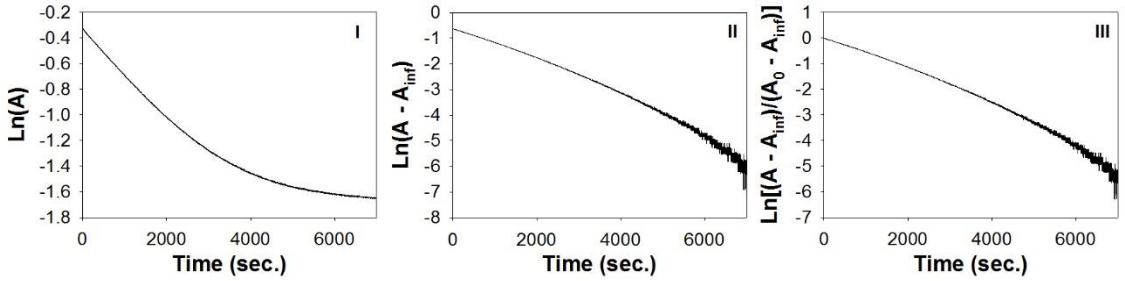

Figure 6 Plots of Equations 4 (I), 11 (II) and 12 (III) for the thermal decay of **SP4**

As can be seen in Figure 7, there is significant variation between plots of Equation 4 and Equations 11 and 12. In the case of the plot of Equation 4, it's clear that the decay in the absorbance of the MC species is not a simple first-order reaction. The plots of Equations 11

and 12 also show curvature, but both equations are identical algebraically with Equation 12 being different only in that the natural log of the *normalized* difference in absorbance per unit time is given. The curvatures of each plot are identical. It can also be seen that as $(A_t - A_{inf})$ approaches zero, the data begins to jump significantly and the plot broadens toward longer times. This negates the necessity of observing the reaction all the way to equilibrium and will significantly alter the regression results of the plot. These observations led to the choice of Equation 11 for all subsequent kinetic regressions contained herein and a timescale for observation of the MC to SP interconversion of ~2000 seconds. The effect of guessing the equilibrium absorbance value (A_{inf}) incorrectly on the linearity of plots of Equation 11 was also investigated and are graphically shown in Figure 7.

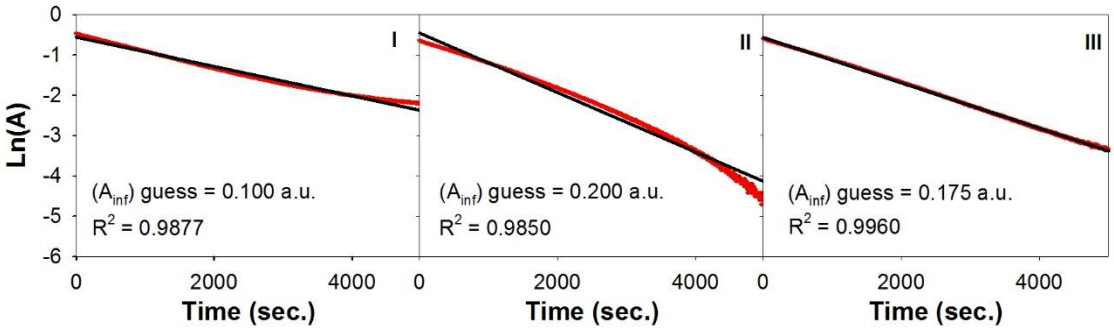

Figure 7 Plots of Equation 11 for **SP4** using low (I), high (II) or correct (III) values of (A_{inf})

Figure 7-I shows that a value for (A_{inf}) that is too low results in a concave-up curvature to the plot and an inaccurate regression result. Figure 7-II shows that guesses for (A_{inf}) that are too high result in a concave-down curvature also giving an inaccurate regression result. Using the appropriate value for (A_{inf}), obtained experimentally for Figure 7-III results in a very straight line with an accurate regression result. Of particular importance to the results presented herein is that the values determined through least-squares linear regression for

($A_0 - A_{inf}$) from the ordinate intercept are physically meaningless due to the fact that it is impossible for one to quantify the molar absorptivity of the MC isomers due to low quantum yields for the photochemical SP to MC interconversion with UV irradiation.

Table 1 Concentrations, rate constants, (Ainf) values, coefficients of determination and experimental wavelength maxima for the thermal MC to SP interconversion process according to least-squares linear regression of five kinetic trials for **SP4** and **SP4-NP** in ethanol at 23 °C according to Equation 11.

System	Concentration ($M \times 10^{-4}$)	k_{obs} ($\times 10^{-4}$ s^{-1})	A_{inf}	R^2_{avg}	λ_{max} (nm)
SP4-NP	1.54 ± 0.01	5.80 ± 0.36	0.175 ± 0.005	0.997	551
SP4	0.695 ± 0.001	5.73 ± 0.05	0.300 ± 0.011	0.999	548

The average regression coefficient (R^2), average observed rate constant (k_{obs}), the maximum wavelength values for each system (λ_{max}) the average equilibrium absorption values and the gravimetrically or thermogravimetrically determined solution concentrations are given in Table 1 for a total of five kinetic trials for each system. An example of an experimental regression of the kinetic data according to Equation 11 is shown in Figure 8 for **SP4** and **SP4-NP**.

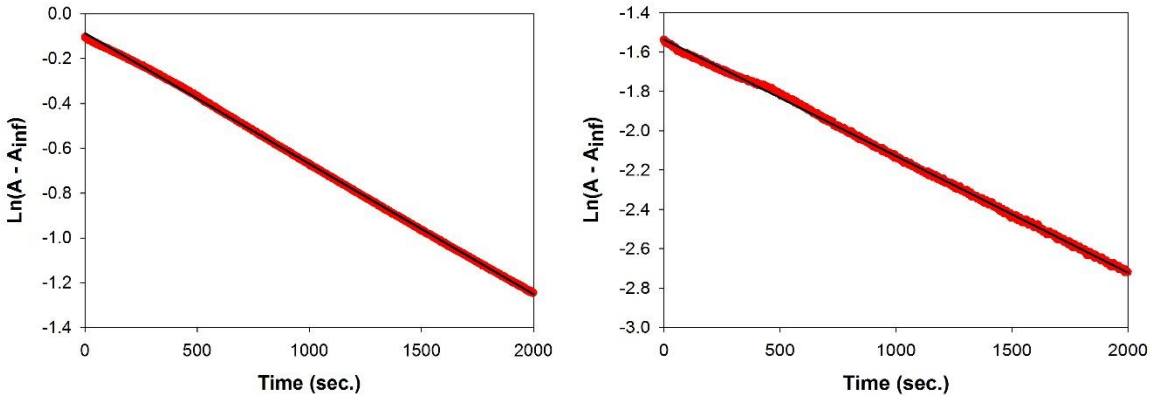

Figure 8 Examples of regression analysis for **SP4** (left) and **SP4-NP** (right) according to Equation 11.

The observed rate constant for the **SP4**-**NP** system is nearly identical to that of **SP4** indicating that the silica/solvent interface has no effect on the thermal interconversion process. Overall, the effect of tethering spiropyran to a silica nanoparticle has implications on only the equilibrium of the system, forcing the conditions for equilibrium to a minimum value of MC concentration.

Due to the variety of integrated rate equations, when this system was first investigated, curvature in the plot of Equation 2 for each trial resulted in a concave-up character seen for the plot that mistakenly led to the idea that traditional first-order kinetic behavior of these systems was being impeded by a pseudo-stable intermediate structure. This mistake was later realized in further kinetic studies and Figure 8 as well as the values given in Table 1 reflect the true interconversion reaction. Nevertheless, mistakes sometimes lead to discovery and the IM-MS investigation in the next section clearly shows that even though the kinetic behavior of spiropyran was misinterpreted according to the wrong integrated rate law, a pseudo-stable intermediate may well occur during MC to SP thermal interconversion.

IM-MS Investigations of **SP1**-**3**

The results of IM-MS experimental investigations of **SP1**-**3** are summarized in Figure 9 as normalized chromatographs of percent relative intensity vs. drift time (t_d) for equilibrated and irradiated solutions. IM-MS experiments provide a wide range of data about the conformation of a system of molecules with the same molecular weight but different geometric shapes in addition to traditional mass spectrometry data.

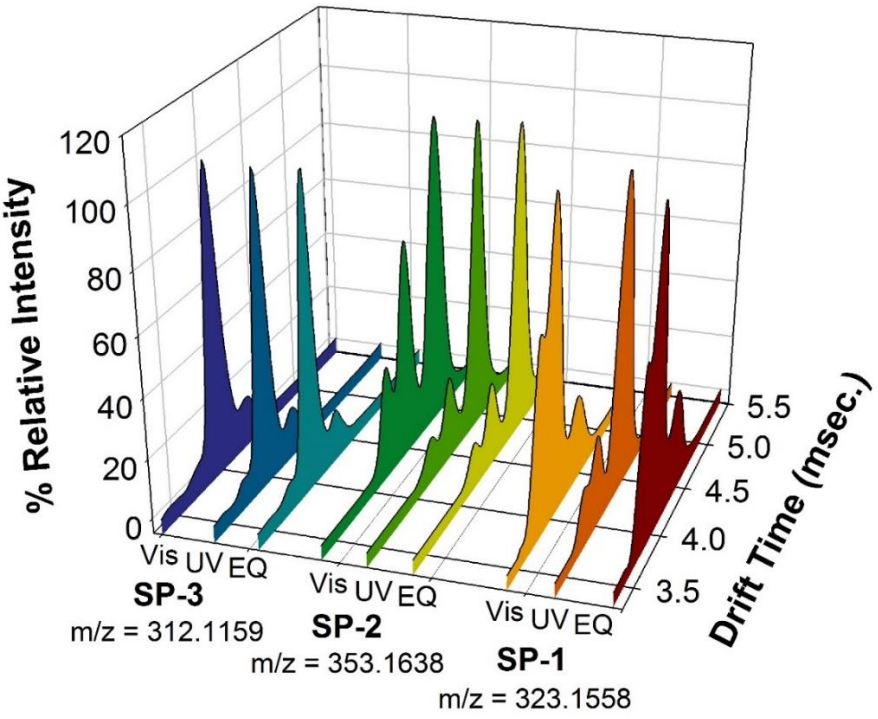

Figure 9 Summary of IM-MS results for **SP1**-**3** in equilibrated and irradiated states

Clearly visible are three singly-charged monomer peaks (confirmed by consideration of the isotopic patterns in the mass spectra of each peak) associated with three different isomeric species for all derivatives studied. UV and visibly irradiated solutions near their PSS's are plotted alongside the equilibrated solution for comparison of light-induced changes in isomer population. For **SP1** and **SP2**, irradiation with UV light causes a significant change in the conformer distribution easing assignment of the last peak to the XTX isomer group. The first two chromatographic peaks with smaller (t_d) values are more difficult to assign conclusively because their populations increase and decrease in a concerted fashion with irradiation. The drift times, semi-quantitative isomer populations (which assume similar ionization efficiency across all seven potential isomers) from deconvolution of the chromatographs and the (R^2) values for each deconvolution are summarized in Table 2.

Table 2 Summary of drift times, mole fractions (x) of each conformer group and coefficients of determination for deconvolution of IM-MS chromatographs. All deconvolutions assume Gaussian shaped peaks for each of three conformer groups for **SP1-3** in IM-MS experiments.

Compound	Peak	Drift Time (msec.)	x_{EQ} (*a*)	x_{UV} (*b*)	x_{VIS} (*c*)	R^2 (*d*)
SP1	1	3.749	0.15	0.08	0.20	0.99975
	2	3.969	0.64	0.12	0.64	
	3	4.410	0.21	0.80	0.16	
SP2	1	4.177	0.06	0.07	0.12	0.99916
	2	4.449	0.14	0.16	0.31	
	3	4.883	0.80	0.77	0.57	
SP3	1	3.601	0.03	0.03	0.03	0.99895
	2	3.809	0.83	0.84	0.80	
	3	4.155	0.14	0.13	0.17	

(a) Mole fractions of each conformer group in equilibrated solutions of **SP1-3**.
(b) Mole fractions of each conformer group in UV irradiated solutions of **SP1-3.**
(c) Mole fractions of each conformer group in visibly irradiated solutions of **SP1-3.**
(d) Coefficient of determination for each deconvolution fitting routing.

In general, the difference in drift times of peaks 2 and 3 are approximately 1.4 – 2 times larger than the difference between peaks 1 and 2. To identify the isomeric species responsible for peaks 1 and 2, computationally aided isomer assignment of the peaks was necessary. CCS values based on DFT-B3LYP optimized geometries are presented in Table 3.

It is clear that the XTX isomer group has the largest CCS values in all cases, but depending on the method, the projection-approximation (PA) or the trajectory method (TJ), the values for the SP, CCC and CCT isomers are not decisive. For this reason, the first two chromatographic peaks for **SP1-3** are only assigned qualitatively to the SP-CCX group of isomers, though we speculate that the second peak is the CCX isomer group based on our CCS calculations.[23] Appendix A contains the mass spectra of each chromatographic peak for equilibrated solutions of **SP1-3**.

Table 3 Theoretical collision cross-sections of **SP1**-**3** based on the projection approximation (PA) and trajectory (TJ) methods provided by the program MOBCAL using DFT-B3LYP energy minimized geometries for seven spiropyran isomers.

	SP1		SP2		SP3	
Isomer	**PA**	**TJ**	**PA**	**TJ**	**PA**	**TJ**
SP	113.30	113.27	120.66	122.69	115.54	111.74
CCC	114.63	117.45	122.57	124.13	116.82	114.48
CCT	112.76	113.57	121.50	122.35	114.86	112.78
TTC	119.38	118.55	128.24	127.28	121.54	115.85
CTC	119.71	118.29	128.63	128.27	121.96	116.37
TTT	119.46	117.83	128.33	126.56	121.58	115.38
CTT	119.56	117.97	128.36	127.48	121.82	116.07

Our data argues for the presence of a CCX isomer group and is the first report of the experimental observation of CCX isomers on timescales greater than nanoseconds. It should be noted that the projection approximation method used here is better than the trajectory method for this particular instrument, which uses an N_2 buffer gas in ion mobility separation whereas the trajectory method specifies a helium buffer gas, though differences between the two buffer gases have been found to be negligible from a qualitative standpoint, even when considering the polarizable character of N_2 gas.[61]

Isomer-Specific Rate Constants of the Thermal MC to SP Interconversion and Computationally Determined Absorption Band Assignments for **SP1**, **SP2** and **SP4**

The results of computational absorption band prediction for each isomer species studied; SP, CCC and XTX, are provided in tabulated form in Appendix B for ZINDO and

TDDFT methods along with their structural energies, relative ranking of stability, frontier orbital transitions, oscillator strengths and wavelength maxima.

Examples of visual representations of predicted absorption maxima and oscillator strengths alongside experimental plots of $(A - A_{inf})$ at the UV PSS and after thermal interconversion has occurred for at least on half-life and are shown in Figures 10 and 11 for the ZINDO and TDDFT results pertaining to **SP2**. Similar Figures for **SP1** and **SP4** in addition to standalone experimental PSS spectra for **SP1**, **SP2** and **SP4** may be found in Appendix B. The reason for plotting the experimental spectra as $(A - A_{inf})$ vs. wavelength is to selectively identify the dynamic bands of the spectrum upon UV irradiation and after at least one half-life of thermal interconversion. TDDFT/CPCM provides the best results in all cases.

The oscillator strengths are plotted in Figures 10 and 11 on the same intervals as the absorption spectra but note that the magnitude of each oscillator strength is actually equated to the area of an absorption band with a maximum absorbance at the predicted maximum wavelength.[62] Because the contributing

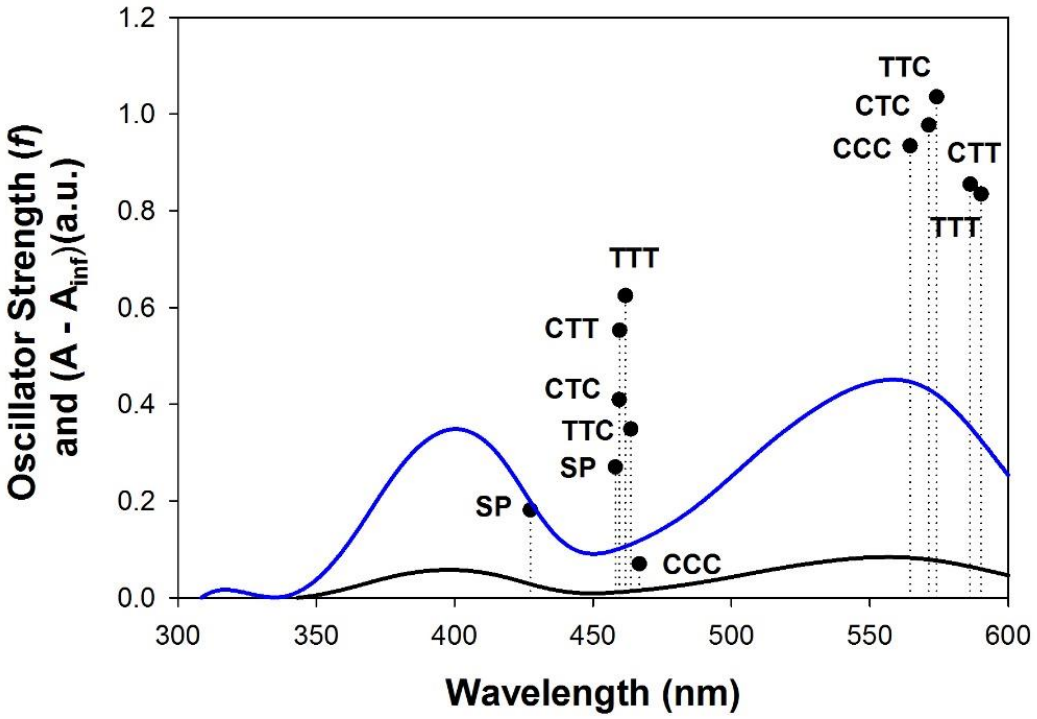

Figure 10 ZINDO/CPCM wavelength maxima, oscillator strengths and experimental spectra for **SP2**

factors to broadening may only be speculated without a much more in depth study of these systems, deconvolution of the experimental spectra into constituent underlying bands would be arbitrary at best. For this reason the reported oscillator strengths from the computational approaches presented are considered only from the perspective that the oscillator strength value is related to the population of each isomer giving rise to the experimental spectra and only a qualitative assignment of isomers to absorption peaks in the experimental spectra are provided.

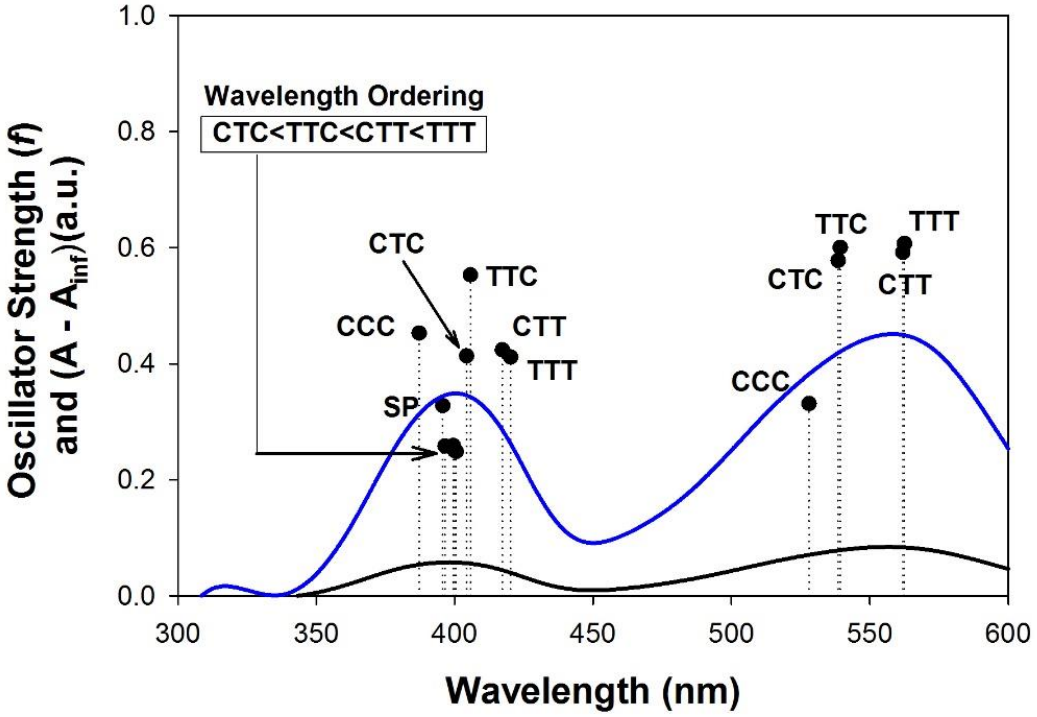

Figure 11 TDDFT/CPCM wavelength maxima, oscillator strengths and experimental spectra for **SP2**

Table 4 Average rate constants for non-shifting peaks, solution concentrations, average coefficients of determination, average (Ainf) values, maximum wavelengths and wavelength maxima shifts during thermal interconversion of MC to SP.

Compound	Concentration ($M \times 10^{-3}$)	k_{obs} ($\times 10^{-3}$ s^{-1})	A_{inf} (a.u.)	R^2_{avg}	$\lambda_{max,1}$ (nm)	$\lambda_{max,2}$ (nm)	$\Delta\lambda_{max}$ (nm)
SP1	2.99 ± 0.01	1.80 ± 0.09	0.126 ± 0.001	0.999	376	541	~4 (541)
SP2	7.03 ± 0.28	18.9 ± 0.1	0.260 ± 0.004	0.999	402	558	~7 (402)
SP4	5.41 ± 0.06	2.48 ± 0.01	0.273 ± 0.009	0.999	376	534	~3 (534)

The rate constant values for **SP1**, **SP2** and **SP4** are reported for the peaks at 376, 376 and 558 nm.

The average kinetic rate constant values (according to Equation 11) for the non-shifting peak, solution concentrations, average coefficients of determination, average (A_{inf}) values, maximum wavelengths and wavelength maxima shifts during thermal interconversion of MC to SP are summarized in Table 4. One peak in the spectra of each compound exhibits a time-dependent shift in maximum wavelength during the thermal interconversion from MC

to SP necessitating kinetic analysis of the peak with no shift in maximum wavelength. The values of (k_{obs}) pertain to the peak where $\Delta\lambda_{max} \approx 0$ nm in Table 4. The results of the kinetic regression analyses are reported in Table 7. Overall, the relative rate constant values for the thermal MC to SP interconversion are **SP2** ≈ (10x) **SP1** ≈ (5x) **SP4**.

IV. DISCUSSION

Thermal Reaction Kinetics of a Spiropyran in Solution and Surface-Bound to a Particle Suspended in Solution

Kinetic analysis of **SP4** and **SP4**-**NP** in ethanol provide insight into the interfacial effects of an amorphous silica nanoparticle/solvent interface on the thermal MC to SP interconversion pathway. The experimentally determined rate constants for thermal MC to SP interconversion are nearly identical as shown in Table 1. This implies that the interfacial region, in which the **SP4** moiety of the **SP4**-**NP** system resides, has a negligible effect on the kinetic behavior of the thermal MC to SP interconversion. Consideration of the PSS spectra for both **SP4** and **SP4**-**NP** systems does, however, indicate that the equilibrium of the **SP4** moiety for the **SP4**-**NP** system could be affected by the interfacial microenvironment.

Solvent effect investigations of spiropyrans have shown that in more polar microenvironments the stability of the MC isomers is much greater than for non-polar microenvironments.[23,63–65] According to these previous investigations, the equilibrium of the **SP4**-**NP** system would lie further toward MC than in the solvated system of **SP4** alone if the polar silica nanoparticle surface was strongly interacting with the surface-bound spiropyrans. This would result in an increase in the equilibrated absorbance of the visible region wavelength maximum for **SP4**-**NP** compared with that of **SP4**. This is apparent at first glance when considering the equilibrated spectra of both systems (Figure 5) but it is difficult, however, to justify that the observed absorbance increase is due to surface-chromophore interactions. Nanoparticle suspensions cause a degree of light scatter that must be considered if the

refractive index (n_D) of the solvent is not an exact match for the nanoparticles. In this case, there is a difference in the visible region refractive index between the silica nanoparticles (n_D = 1.46) and the ethanol solvent (n_D = 1.36).[66] This small difference decreases the efficiency of spiropyran UV irradiation due to light scatter and consequently decreases the quantum yield of the photochemical conversion from SP to MC upon irradiation with UV light. Decreases in probe beam transmission also occur due to light scatter giving a false rise in absorbance. Light scattering effects on irradiation and probe beam transmission are the more likely culprits for the decreased quantum yield in **SP4**-**NP** and higher visible region absorbance of **SP4**-**NP** compared to **SP4**, respectively.

Irradiation of **SP4** in solution with visible light was observed to cause a decrease in absorbance for the visible region peak but the same changes in the spectra of **SP4**-**NP** are not observed. This fact, in addition to the aforementioned light scattering effects caused by slight refractive index mismatching indicate that the lower irradiated sample absorbance difference of the visible region maximum for **SP4**-**NP** is not clearly explained by the experimental spectra. For this reason, the microenvironmental effects of the silica/solvent interfacial region must be inferred from kinetic characterization alone.

The MC isomers have been shown to exhibit both zwitterionic[67] and quinoidal[68] character depending on substituents, solvent and the excited state of the molecule. In polar solvents such as ethanol, zwitterionic character is favored in the ground state and the excited states. The importance of zwitterionic electronic structure to the kinetic characterization presented here is two-fold; (1) the extra lone pair of the oxygen of the *p*-nitrophenolate moiety of the MC isomers are more available for bonding than the quinoidal electronic configuration allows upon thermal reversion back to the SP isomer and (2) the positive and negative charges

on the nitrogen and oxygen, respectively, are able to coordinate with solvent molecules and other MC isomers to stabilize the MC geometry in addition to facilitating charge-transfer interactions between proximal MC molecules. Kinetically, intermolecular **SP4**-**SP4** interaction on the surface of the silica nanoparticles would result in a smaller rate constant for thermal MC to SP interconversion, due to charge transfer interactions as a result of zwitterionic character or spiropyran aggregate formation between proximal surface-bound chromophores.

Two aggregation motifs have been theoretically studied for spiropyrans containing long hydrocarbon N-substituents (indole); J- and H- aggregates.[69] J-type aggregates are characterized by end-to-end charge-transfer interactions whereas H-type aggregates are characterized by stacking charge-transfer interactions. Though generally weak for both systems studied without considering solvent interactions (> -5 kcal mol^{-1} for both aggregate types), the presence of water causes an increase in interaction strength favoring J-aggregation (-13.7 kcal mol^{-1}) over H-aggregation (-9.2 kcal mol^{-1}). If either aggregation motif occurs on the surface of the particle, it has little to no effect on the kinetic behavior of the system and can be ruled out based on our experimentally determined rate constants.

Nanoparticle aggregation has also been known to affect the stability of suspensions of spiropyran nanoparticles; when they are irradiated with UV light, spontaneous particle aggregation can occur resulting in sedimentation and false decreases in the absorbance spectrum of the suspension.[14] Nanoparticle aggregation in our system, however, was not observed throughout kinetic analysis experiments, most likely due to continued agitation of the suspension while monitoring thermal MC to SP interconversion. Due to the aforementioned knowledge of spiropyran J- and H- aggregation, electronic character and nanoparticle aggregation we argue that effect of silica on the spiropyran reaction, assuming no nanoparticle aggregation upon UV irradiation of **SP4**-**NP**, is only realized as a decrease in the

quantum yield of the photochemical SP to MC interconversion, but does not significantly affect the thermal kinetic behavior of the system.

IM-MS Investigations of **SP1-3**

IM-MS experiments using **SP1-3** have resulted in the observation of three isomeric groups of conformers on millisecond timescales. Previously reported lifetimes for the XTX isomers are in the range of milliseconds and for the CCC isomer in the range of picoseconds.[70] These previously reported lifetimes are also supported by other investigations using NMR,[33,71–76] time resolved emission spectroscopy,[71] theoretical approaches[23,77] and transient absorption studies.[78–80] Our investigations, however, contradict some of these previously reported lifetimes and are more closely aligned with those reported in other transient absorption studies that also contradict those already noted.[64] Specifically insofar as the *cis* → *trans* isomerization on the photochemical pathway is on the order of micro to milliseconds.

The reported photochemical excited state isomerization rate[64] should occur much faster than the thermal ground state *trans* → *cis* isomerization studied here and our observation of what we believe to be the *cisoid* MC isomers, namely the CCC, may not be a reflection of their stability but a reflection of *instantaneous* population of the CCX isomers. This is evidenced by the thermal reaction equation, MC ⇌ SP, identified as the most accurate assessment of thermal kinetic behavior by our empirical approach (Figures 6 and 7). Also of notable mention is that the MC isomers, when protonated at the phenolate oxygen are unlikely to revert to the SP isomer as quickly as unprotonated MC isomers as indicated by computational stability studies of MC isomers thermal ionization processes such as that encountered in ESI

protonation.[81]

Many of the previously reported lifetimes for the CCX and XTX isomer groups have approached the spiropyran system frequently using simplified models of the *photochemical* reaction pathway and relatively little experimental evidence for the parent spiropyran systems have been presented, other than conventional kinetic characterization and transient absorption studies, for the thermal reaction pathway. Because our IM-MS experiments reflect a collection of parent spiropyran systems that are thermally equilibrating up to the moment of transfer into the gas phase, photochemical data also may not be appropriate for comparison with our results. To our knowledge, only one experimental gas phase study has been performed for the spiropyran system which utilized photoelectron spectroscopy and transient absorption pump/probe techniques to examine the gas-phase dynamics of spiropyran photochemical interconversion.[82] Their results indicated that the photochemical excitation resulted in the formation of a TCC intermediate, but theoretical investigations[23] and the results of our own computational modelling have shown that spiropyrans with a dimethyl substituent on the indole moiety sterically prohibits formation of both the TCT and TCC isomers.

Recent investigations into the solution (thermodynamically controlled) → gas-phase (kinetically controlled) transfer processes of biomolecules using ESI ionization methods have argued that solution structure is preserved upon transfer into the gas phase.[83–85] Also, the effect electric fields, encountered by the species of interest in mass spectrometry experiments, has been studied[63] and shown to favor SP isomer ring-opening, though the effects of the electric field are less significant than protonation; a requisite condition for mass spectrometric analysis. Consequently, if one is willing to entertain the idea that the geometric structure of spiropyran systems is preserved in IM-MS experiments and that protonation of MC isomers significantly stabilize them, these results present a unique viewpoint into the geometries and mechanistic

behavior of spiropyrans in general. Specifically, the photodegredation of spiropyrans that prevent their application as photoswitches could be due in large part to the instantaneous formation of a biradical upon cleavage and reformation of the spirocarbon-oxygen bond as evidenced by our postulated observation of a *cisoid* MC isomer group in IM-MS experiments.

Prior to suggesting any mechanism for the thermal MC to SP interconversion, differences in the microenvironment between the solution and gas-phase must be considered. Our observation of an isomeric species other than those within the XTX isomer group and the SP isomer in gas-phase studies in addition to kinetic characterization of the thermal MC to SP interconversion as a first-order equilibrium process lends credence to the fact that the CCC and CCT isomers may not be ruled out as significant contributors to the kinetic behavior of spiropyrans on timescales greater than milliseconds and their resultant potential for susceptibility to photodegredation. We postulate, however, that the thermal MC to SP interconversion proceeds through a long-lived or significantly present instantaneous *cisoid* intermediate structure that may or may not be observable in conventional absorbance spectroscopy studies.

Isomer-Specific Rate Constants of the Thermal MC to SP Interconversion and Computationally Determined Absorption Band Assignments for **SP1**, **SP2** and **SP4**

ZINDO and TDDFT studies presented herein represent an attempt to determine which of six major isomeric species (CCC, CTT, CTC, TTC, TTT and SP), identified based on IM-MS computational structural assessments, of the spiropyran system give rise to the experimental absorption spectra of **SP1**, **SP2** and **SP4**. Solvent modeling was used to provide

a more accurate assessment of the solvent (methanol) interaction through the CPCM model thereby justifying comparison of the predicted spectra to experimental spectra which also used methanol solvent. All geometries were optimized at the DFT-B3LYP level of theory using a lower level basis set than IM-MS modeling (6-31G++(d,p) for absorption prediction vs. 6-31G++(d',p') for IM-MS modeling) because computational expense was of no concern for this work.

Both basis sets have been shown to provide good agreement with experimentally obtained geometries and the differences may be negligible, but overall a higher level of theory generally results in more accurate prediction of molecular geometry, particularly when the appropriate solvent model is used.[86] It should be noted, however, that hydrogen-bonding interactions of methanol and the various spiropyran isomers are not considered when using the CPCM model. Explicit solvent modelling has shown that only a few water molecules are enough to stabilize the merocyanine isomers.[63] A visual assessment of the predicted wavelength maxima and oscillator strengths with the experimental spectra (Figures 10 and 11) for **SP1**, **SP2** and **SP4** clearly justify the claim that the TDDFT approach used here is much more consistent with the experimental spectra and isomer assignments have been made using only this approach.

For **SP1** the peak centered at 541 nm appears to be the result of an overlap of two spectral bands, as indicated by the shift in maximum wavelength and the presence of asymmetry in the band. Comparing the TDDFT results to the experimental spectra indicates that the XTT isomers are predominantly responsible for this convoluted band but the energies of the isomers would suggest that it is only the TTT and TTC isomers which contribute. For the peak centered at 376 nm, all of the isomers in the XTX group have similar oscillator strengths and absorption maxima, except for the SP isomer and CCC isomer which do not

correlate well with either peak. The TTC and CTC isomers have two predicted absorption bands near 376 nm, whereas all others only display one predicted band. As a result, the kinetic rate constant value reported may be tentatively assigned to the TTX isomer group but further investigation is necessary to conclusively make this claim and so, for the purposes of this study, must be considered the XTX isomer group.

SP2 exhibits unique differences compared to that of **SP1** and **SP4**. Main differences are that the peak which shifts as the MC to SP thermal interconversion occurs is reversed, and is the peak centered at 402 nm. In terms of the energy and predicted maxima, the peak centered at 558 nm is most likely the convoluted band of two overlapping constituent peaks as well, but the lack of a shift in wavelength with time is peculiar. The correlation of the TTC/CTC and TTT/CTT isomers with the shoulder and peak of this band, respectively, are also very similar to **SP1** except that lack of a time dependent shift in this peak indicates either a concerted decay of the separate underlying absorption bands or caused by an experimental artifact. The CCC predicted maximum for the peak at 558 nm is close to the predicted maxima of the TTC/CTC isomer group though its calculated energy relative to all other isomers considered is the highest and it is unlikely that it contributes to the observed spectrum. The peak centered at 402 nm is also similar to that of **SP1** in that a concentration of all XTX isomers in addition to a predicted band for SP and CCC is predicted, but again, this decrease in absorbance of this peak as time progresses along the thermal MC to SP interconversion negates the assignment of this peak to the SP isomer. The TTC isomer exhibits two predicted absorption maxima very near the experimental maximum of 402 nm with one having the highest oscillator strength for this peak. The reported rate constant for **SP2** is based on the decay of the peak at 558 nm and can be attributed to the XTX isomer group for the same reasons provided for **SP1**, except that all specific XTX isomers contribute nearly equally to

the observed band according to the predicted results.

SP4 absorbance spectra prediction represents an analogous situation to that of **SP1.** Very similar absorption maxima and oscillator strengths were calculated. The reported rate constant for **SP4** pertains to the peak at 376 nm and can only be assigned to the XTX isomer group. One difference between the predicted spectra of **SP1** and **SP4** is that the predicted absorption bands for the peak at 376 nm for all XTX isomers are very similar both in terms of oscillator strength and wavelength maxima. These reasons invalidate any tentative assignment of the reported rate constant for **SP4** to a more specific isomer group other than the XTX group.

Kinetic analysis results are similar to those reported in the first portion of the work for the **SP4** and **SP4-NP** systems in ethanol at 23 ºC. The rate constants of thermal MC to SP interconversion for **SP1** and **SP4** are relatively close and that of **SP2** is approximately one order of magnitude greater than that of **SP1**. The reason for performing these kinetic trials in methanol was an attempt at observing any deviation from first-order behavior according to Equation 11 that may be occurring as a result of the previously determined millisecond lifetimes of the *cisoid* MC isomers in IM-MS experiments, but none was found.

V. CONCLUSIONS

Studies of **SP4** and **SP4-NP** systems in ethanol at 23 C revealed that the microenvironmental effects of chemically modifying amorphous silica nanoparticles with spiropyran moieties has a negligible effect on the overall kinetic behavior of the thermal MC to SP interconversion process. Light scattering effects, nanoparticle and surface moiety aggregation were also noted to potentially inhibit the formation of SP isomers using visible irradiation resulting in a lower quantum yield for the reaction compared with photochemical activity in the solvent system.

IM-MS experiments revealed that protonated *cisoid*-MC isomers may have lifetimes much greater than those reported for solution phase studies. The possibility that phase-transfer from solution to gas using ESI could preserve solution structure further supports our postulate that a long-lived *cisoid* MC was detected in IM-MS experiments and theoretical CCS values substantiate this claim. Absorption band assignments revealed little in the way of pinpointing isomer specific absorption and rate constants but did show that the *cisoid* isomer is unlikely to significantly absorb in the UV-visible region of the electromagnetic spectrum. Post IM-MS kinetic analysis of **SP1**, **SP2** and **SP4** further invalidated the possibility that the *cisoid* isomers play a significant role in solution phase kinetic behavior. Despite these results, the question of how stable an intermediate isomer can be, yet still play an insignificant role in the long timescale behavior of spiropyran is intriguing.

In lieu of the aforementioned effects of protonation and the microenvironment on the geometries and reactivities of spiropyrans and our kinetic

analysis results, we postulate that a phase-dependent mechanism is necessary to explain the noted discrepancies between gas phase and solution phase behavior. Scheme 4 shows both

postulated mechanisms for the thermal MC to SP interconversion with the phase-dependent rate-determining step annotated. Note that the gas-phase mechanism includes a proton located on the phenolate oxygen.

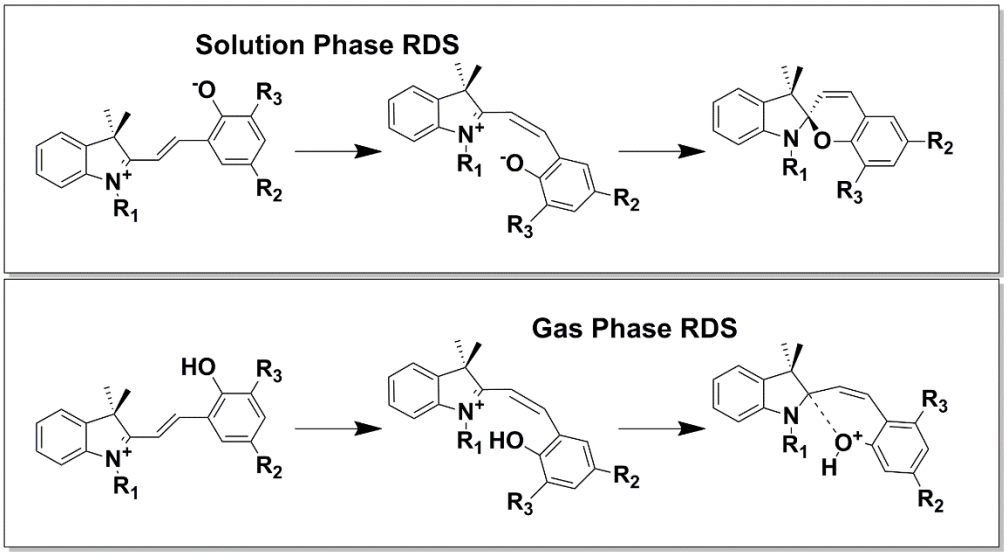

Scheme 4 Postulated phase-dependent thermal MC to SP interconversion mechanisms.

Our postulate observes the proper protonation site according to computational[81] and experimental[33] investigations. In the gas phase, protonation prohibits complete reformation of the spirocarbon-oxygen bond thereby causing a build-up in population of the *cisoid* merocyanine, observed in IM-MS investigations. In contrast, the solution phase rate-determining step must be the *trans*→*cis* isomerization, as noted in other aforementioned investigations. Our kinetic analysis of solution phase thermal MC to SP interconversion also supports this conclusion because the rate-determining step and unlikely UV-visible absorption of the *cisoid* merocyanines according to TDDFT analysis do not support a long-lived intermediate *cisoid* isomer.

The work presented herein is significant to the disciplines of photochemistry, physical chemistry and computational chemistry as it represents a completely original, uniquely

integrated approach to mechanistic studies not previously reported. Mechanisms may be postulated using traditional techniques such as quenching, trapping, NMR, ultrafast spectroscopy and computational studies to name a few, but the approach presented here uses a previously unreported method that combines some of the most advanced aspects of each discipline on conventional timescales. Though the use of ultrafast spectroscopy to study excited states in photochemical systems is widely regarded as revolutionary, it is difficult to ascertain concretely that which one observes. By combining the rapidly advancing field of computational chemistry with traditional physical chemistry (chemical kinetics) and the newly developed analytical and physical technique of IM-MS for small molecules, we have been able to, *for the first time*, observe a challenging, complex photochemical system on conventional timescales providing objective, unambiguous results for the stable and meta-stable isomers of the spiropyran system.

APPENDIX SECTION

APPENDIX A: IM-MS SUPPLEMENTARY INFORMATION

Detailed IM-MS Chromatographs with Mass Spectra for Each Detected Conformer

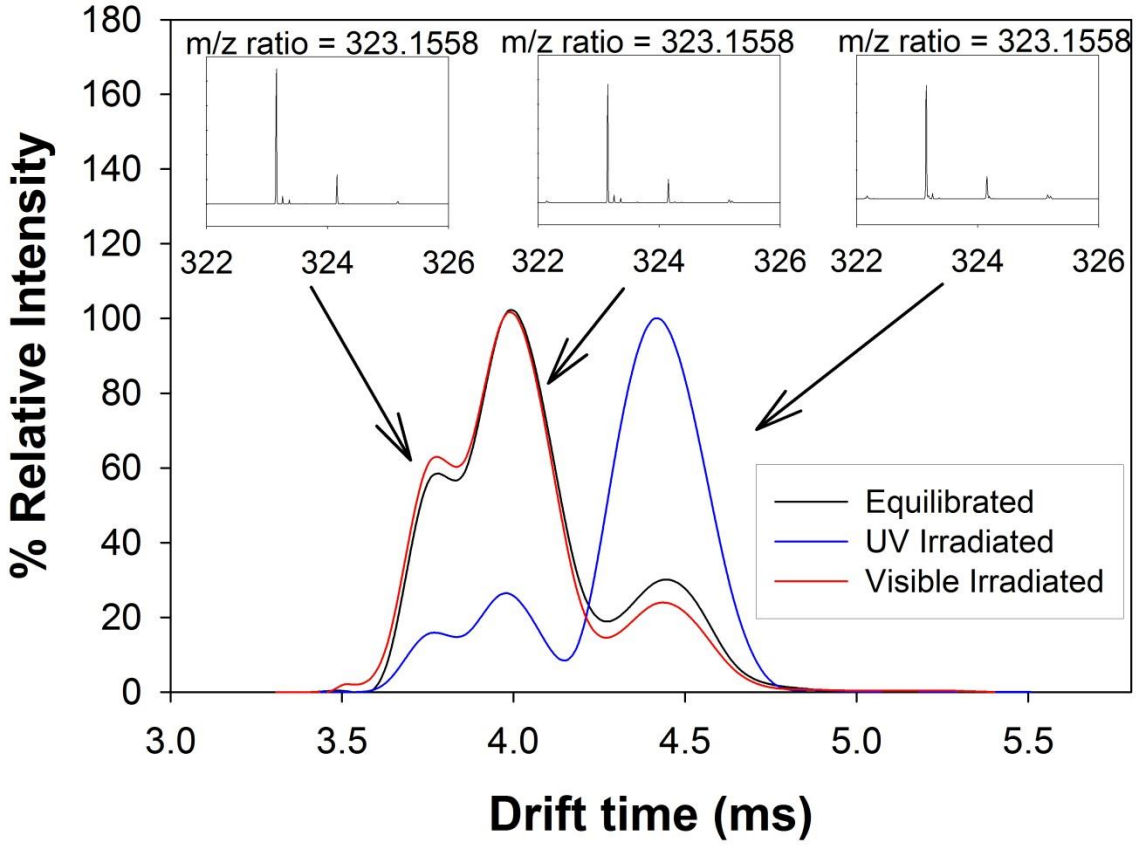

Figure S1: IM-MS Spectra and Chromatographs for **SP1**

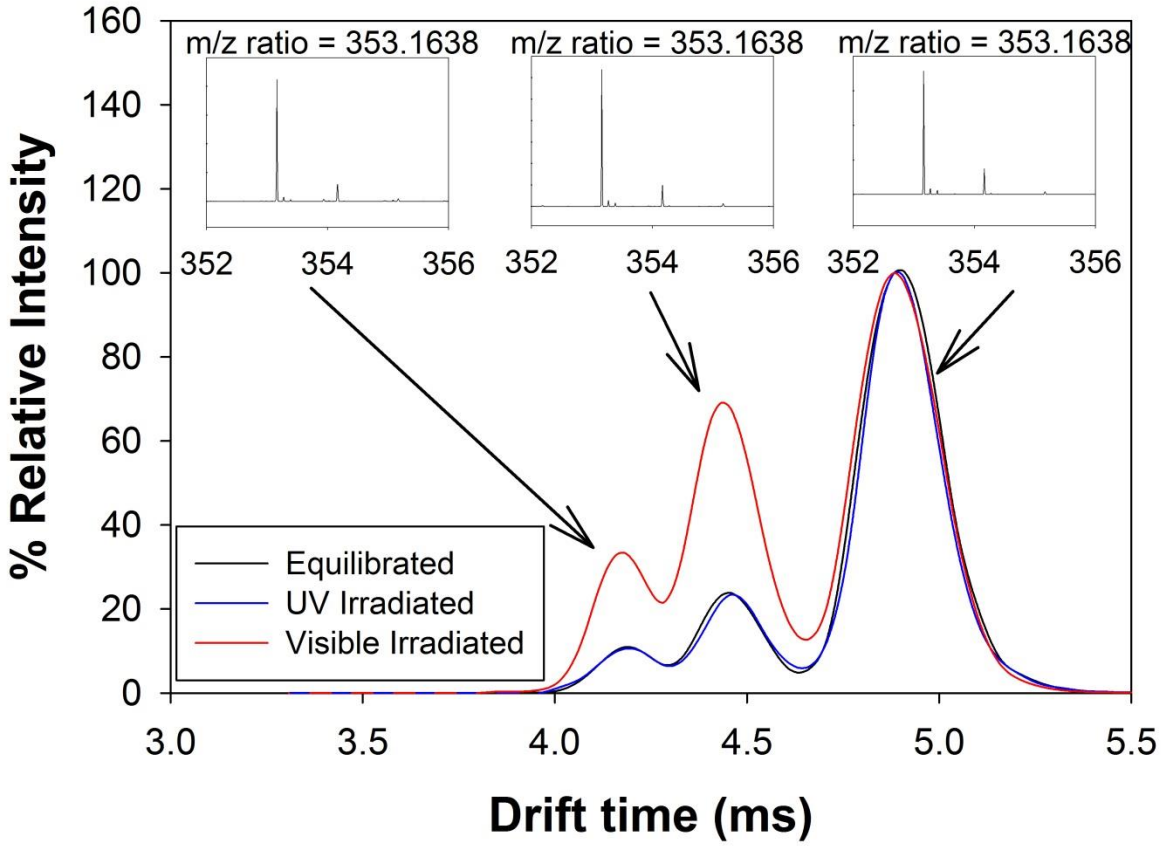

Figure A2: IM-MS Spectra and Chromatographs for **SP2**

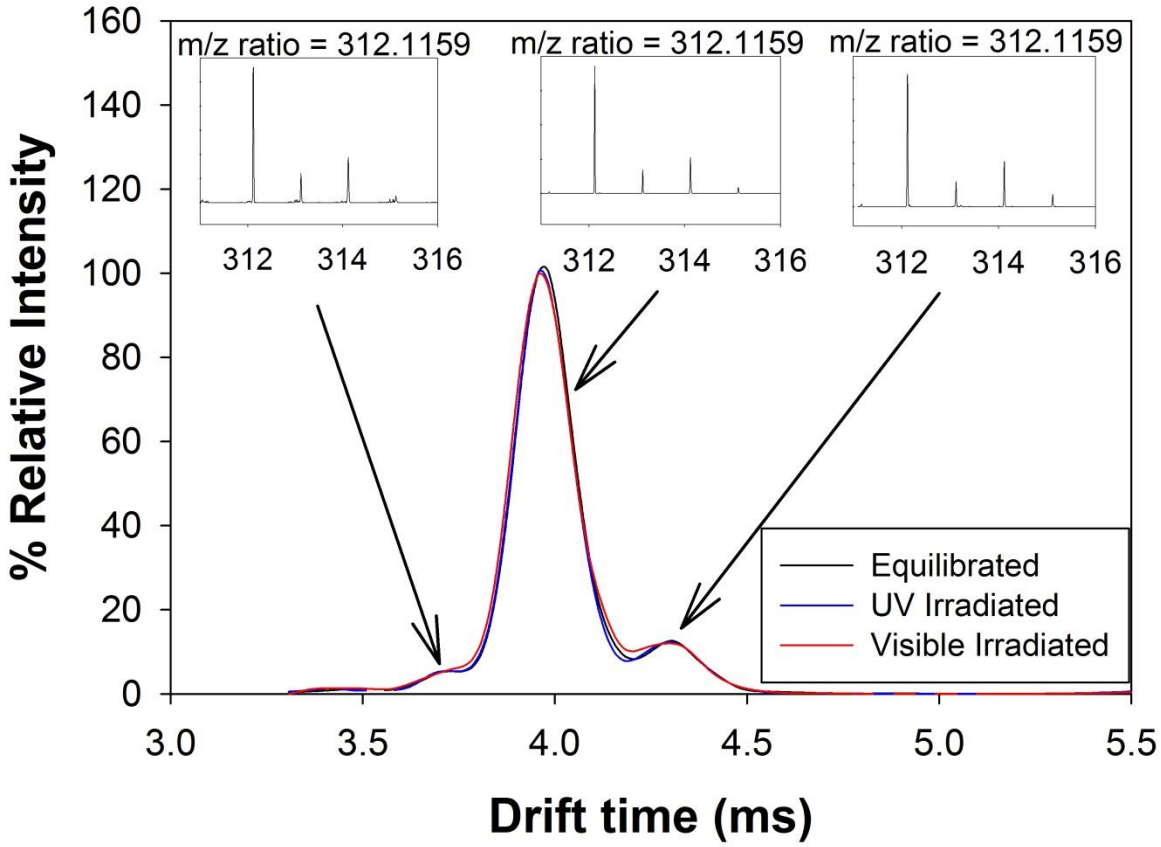

Figure A3: IM-MS Spectra and Chromatographs for **SP3**

APPENDIX B: ABSORPTION BAND PREDICTION SUPPLEMENTARY INFORMATION

ZINDO and TDDFT Absorption Spectra Prediction Plots for **SP1** and **SP4**

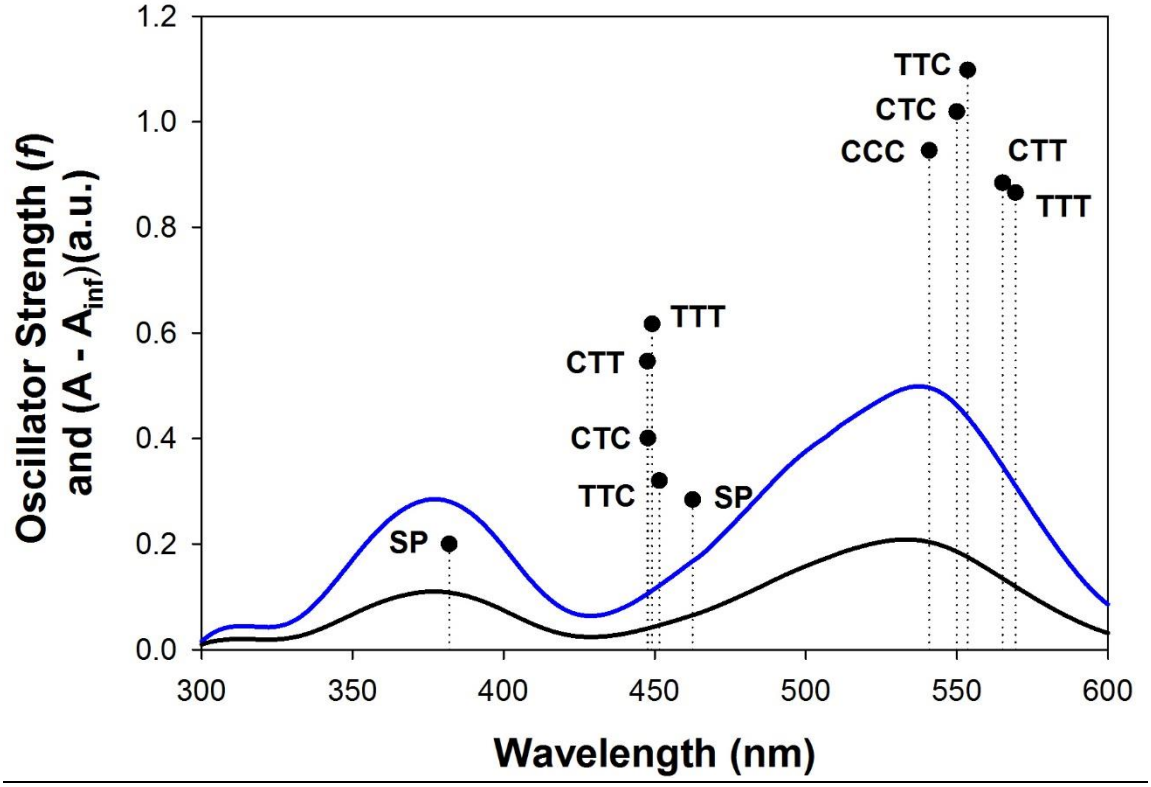

Figure A4 ZINDO/CPCM Predicted and Experimental Spectra for **SP1**

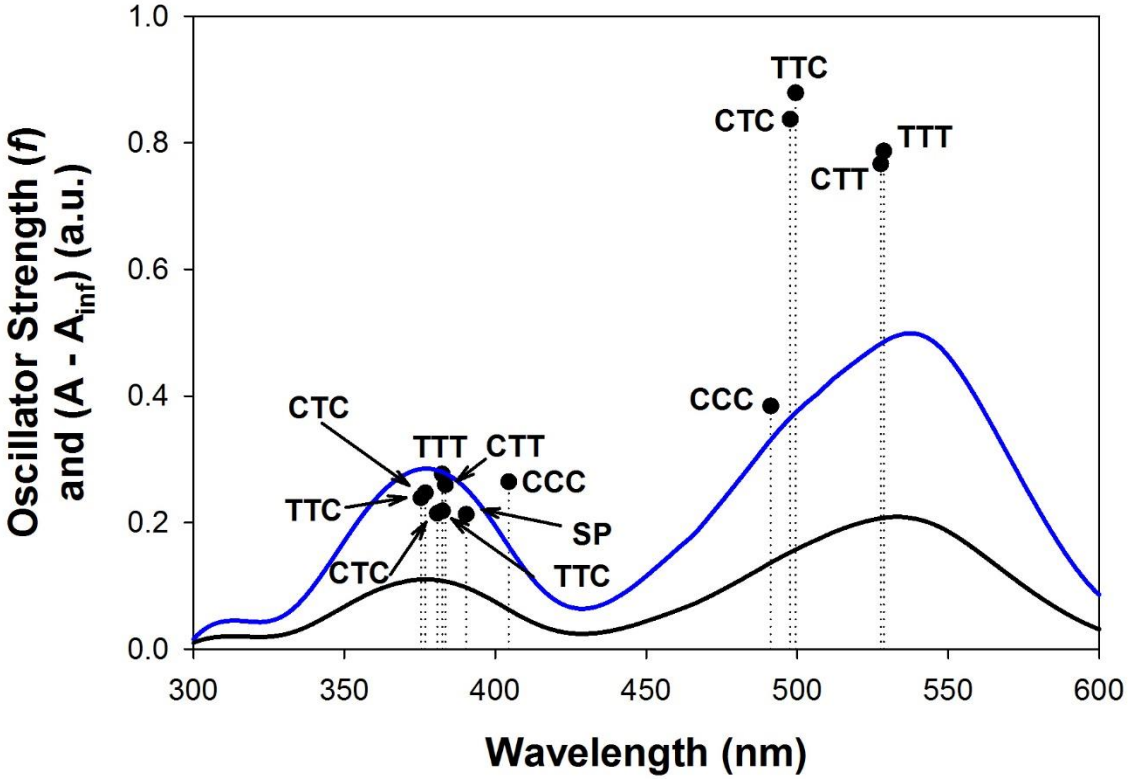

Figure A5 TDDFT/CPCM Predicted and Experimental Spectra for **SP1**

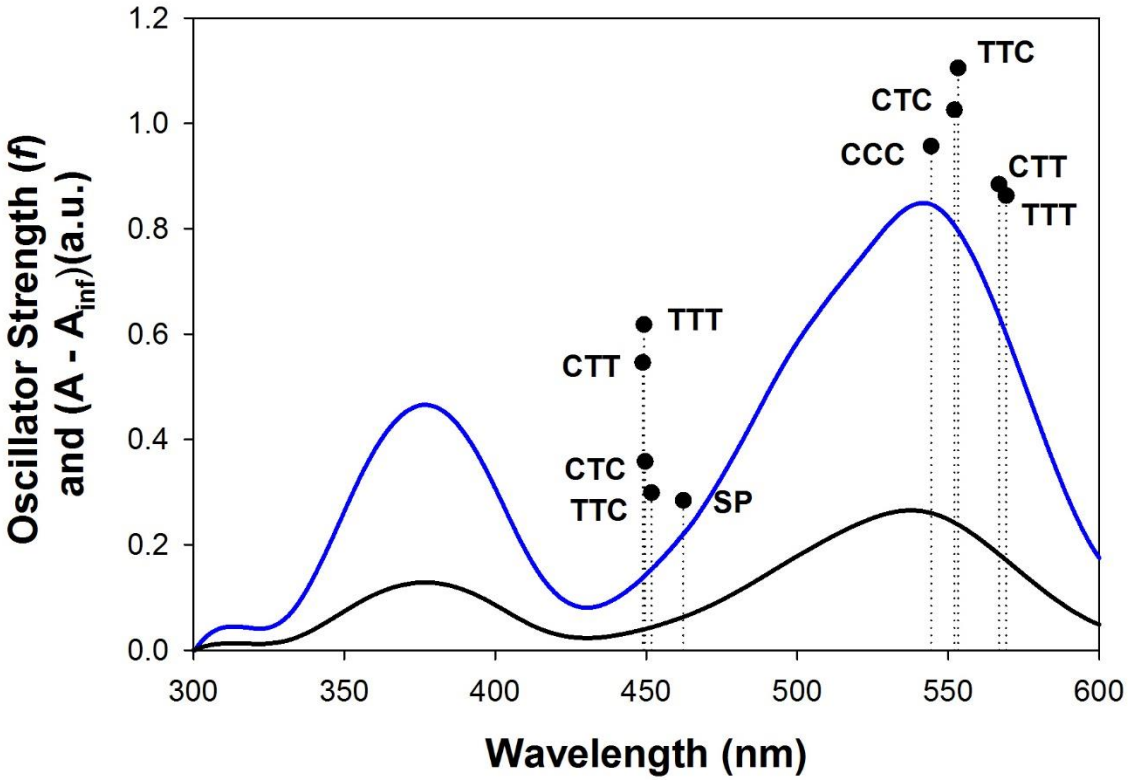

Figure A6 ZINDO/CPCM Predicted and Experimental Spectra for **SP4**

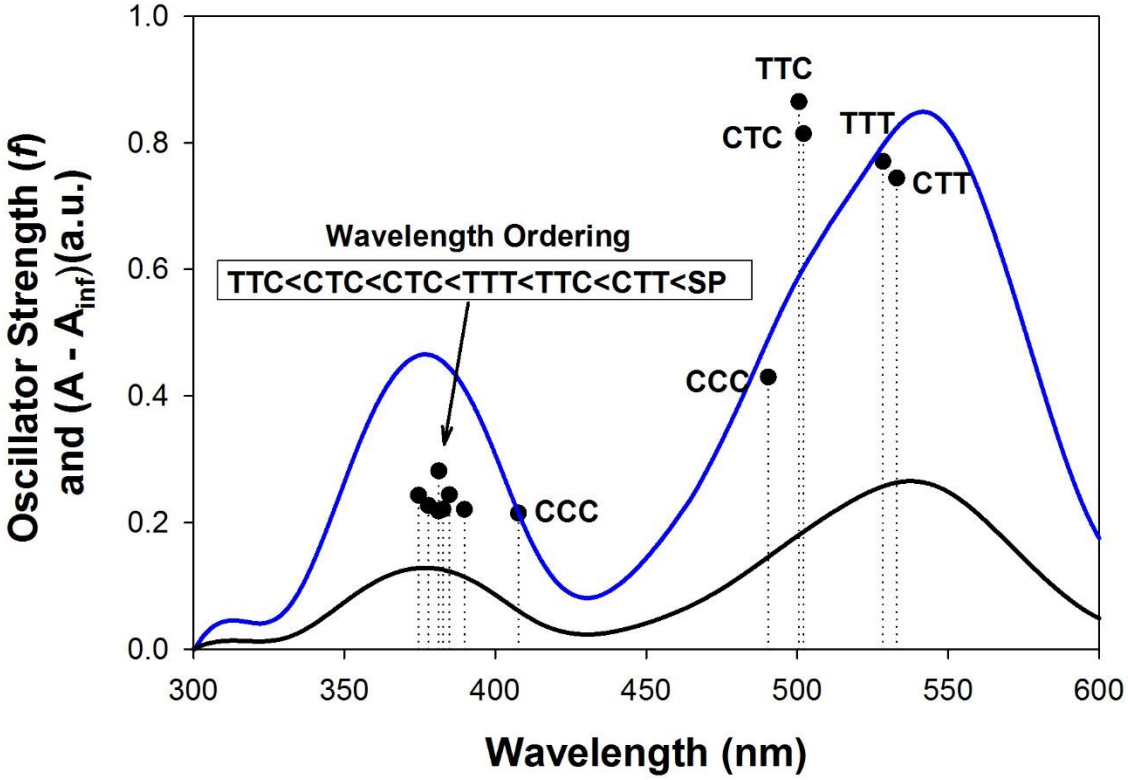

Figure A7 TDDFT/CPCM Predicted and Experimental Spectra for **SP4**

Tabulated Isomer Specific Electronic Absorption Maxima, Oscillator Strengths, Primary Orbital Transitions, Isomer Energies and Relative Stability Rankings for TDDFT and ZINDO Prediction Methods

Table A1 ZINDO/CPCM predicted absorption maxima, oscillator strengths (f), primary orbitals involved in the associated absorption, isomer energies and relative rankings of stability for **SP1**, **SP2** and **SP4**

ZINDO	Isomer	λmax (nm)	f	Primary Transition	Energy (hartrees)	Stability (*a*)
SP1	SP	462.50	0.2841	(HOMO-1) → (LUMO)	-1070.00780793	5
		381.97	0.2002	(HOMO-3) → (LUMO)		
	CCC	540.87	0.9457	(HOMO) → (LUMO)	-1070.00370574	6
	CTC	550.00	1.0191	(HOMO) → (LUMO)	-1070.01373787	3
		447.78	0.4006	(HOMO) → (LUMO+1)		
	CTT	565.13	0.8843	(HOMO) → (LUMO)	-1070.01266433	4
		447.57	0.5462	(HOMO) → (LUMO+1)		
	TTC	553.59	1.0981	(HOMO) → (LUMO)	-1070.01640420	1
		451.51	0.3202	(HOMO) → (LUMO+1)		
	TTT	569.44	0.866	(HOMO) → (LUMO)	-1070.01496054	2
		449.15	0.6171	(HOMO) → (LUMO+1)		
SP2	SP	458.05	0.2703	(HOMO-1) → (LUMO)	-1184.53416663	5
		427.34	0.1816	(HOMO-2) → (LUMO)		
	CCC	564.59	0.9345	(HOMO) → (LUMO)	-1184.53201516	6
		466.69	0.0702	(HOMO) → (LUMO+1)		
	CTC	571.31	0.9772	(HOMO) → (LUMO)	-1184.54210130	3
		459.44	0.4099	(HOMO) → (LUMO+1)		
	CTT	586.31	0.8548	(HOMO) → (LUMO)	-1184.54158019	4
		459.62	0.5530	(HOMO) → (LUMO+1)		
	TTC	574.19	1.0355	(HOMO) → (LUMO)	-1184.54478499	1
		463.67	0.3487	(HOMO) → (LUMO+1)		
	TTT	590.18	0.8348	(HOMO) → (LUMO)	-1184.54390349	2
		461.66	0.6244	(HOMO) → (LUMO+1)		
SP4	SP	462.25	0.2842	(HOMO-1) → (LUMO)	-1264.10318388	5
	CCC	544.35	0.9566	(HOMO) → (LUMO)	-1264.09879639	6
	CTC	552.09	1.0258	(HOMO) → (LUMO)	-1264.10976033	3
		449.60	0.3581	(HOMO) → (LUMO+1)		
	CTT	566.86	0.8845	(HOMO) → (LUMO)	-1264.10872014	4
		448.80	0.5459	(HOMO) → (LUMO+1)		
	TTC	553.26	1.1053	(HOMO) → (LUMO)	-1264.11346972	1
		451.69	0.2987	(HOMO) → (LUMO+1)		
	TTT	569.17	0.8628	(HOMO) → (LUMO)	-1264.11211116	2
		449.25	0.6179	(HOMO) → (LUMO+1)		

Table A2 TDDFT/CPCM predicted absorption maxima, oscillator strengths (f), primary orbitals involved in the associated absorption, isomer energies and relative rankings of stability for **SP1**, **SP2** and **SP4**

TD-DFT	Isomer	λmax	f	Primary Transition	Energy (hartrees)	Stability (*a*)
SP1	**SP**	S(390.37)	0.2127	(HOMO-1) → (LUMO)	-1070.00780793	5
	CCC	S(491.19)	0.3840	(HOMO) → (LUMO)	-1070.00370574	6
		S(404.42)	0.2642	(HOMO-1) → (LUMO)		
	CTC	S(497.68)	0.8369	(HOMO) → (LUMO)	-1070.01373787	3
		S(380.76)	0.2142	(HOMO) → (LUMO+1)		
		S(376.84)	0.2468	(HOMO-1) → (LUMO)		
	CTT	S(527.68)	0.7664	(HOMO) → (LUMO)	-1070.01266433	4
		S(383.52)	0.2593	(HOMO-1) → (LUMO)		
	TTC	S(499.45)	0.8787	(HOMO) → (LUMO)	-1070.01640420	1
		S(382.46)	0.2182	(HOMO) → (LUMO+1)		
		S(375.41)	0.2386	(HOMO-1) → (LUMO)		
	TTT	S(528.69)	0.7867	(HOMO) → (LUMO)	-1070.01496054	2
		S(382.42)	0.2765	(HOMO-1) → (LUMO)		
SP2	**SP**	S(395.68)	0.3275	(HOMO-1) → (LUMO)	-1184.53416663	5
	CCC	S(528.00)	0.3311	(HOMO) → (LUMO)	-1184.53201516	6
		S(387.13)	0.4524	(HOMO-1) → (LUMO)		
	CTC	S(538.55)	0.5775	(HOMO) → (LUMO)	-1184.54210130	3
		S(404.31)	0.4132	(HOMO-1) → (LUMO)		
		S(396.52)	0.2579	(HOMO-2) → (LUMO)		
	CTT	S(561.91)	0.5917	(HOMO) → (LUMO)	-1184.54158019	4
		S(417.20)	0.4235	(HOMO-1) → (LUMO)		
		S(400.04)	0.2499	(HOMO) → (LUMO+1)		
	TTC	S(539.28)	0.6002	(HOMO) → (LUMO)	-1184.54478499	1
		S(405.69)	0.5528	(HOMO-1) → (LUMO)		
		S(399.51)	0.2586	(HOMO) → (LUMO+1)		
	TTT	S(562.54)	0.6069	(HOMO) → (LUMO)	-1184.54390349	2
		S(420.16)	0.4114	(HOMO-1) → (LUMO)		
		S(400.52)	0.2485	(HOMO) → (LUMO+1)		
SP3	**SP**	S(389.80)	0.2207	(HOMO-1) → (LUMO)	-1264.10318388	5
	CCC	S(490.39)	0.4300	(HOMO) → (LUMO)	-1264.09879639	6
		S(407.64)	0.2148	(HOMO-1) → (LUMO)		
	CTC	S(502.10)	0.8143	(HOMO) → (LUMO)	-1264.10976033	3
		S(377.87)	0.2267	(HOMO-1) → (LUMO)		
		S(381.21)	0.2182	(HOMO) → (LUMO+1)		
	CTT	S(532.97)	07443	(HOMO) → (LUMO)	-1264.10872014	4
		S(384.77)	0.2438	(HOMO) → (LUMO+1)		
	TTC	S(500.52)	0.8650	(HOMO) → (LUMO)	-1264.11346972	1
		S(374.56)	0.2430	(HOMO-1) → (LUMO)		
		S(382.72)	0.2210	(HOMO) → (LUMO+1)		
	TTT	S(528.39)	0.7706	(HOMO) → (LUMO)	-1264.11211116	2
		S(381.28)	0.2817	(HOMO-1) → (LUMO)		

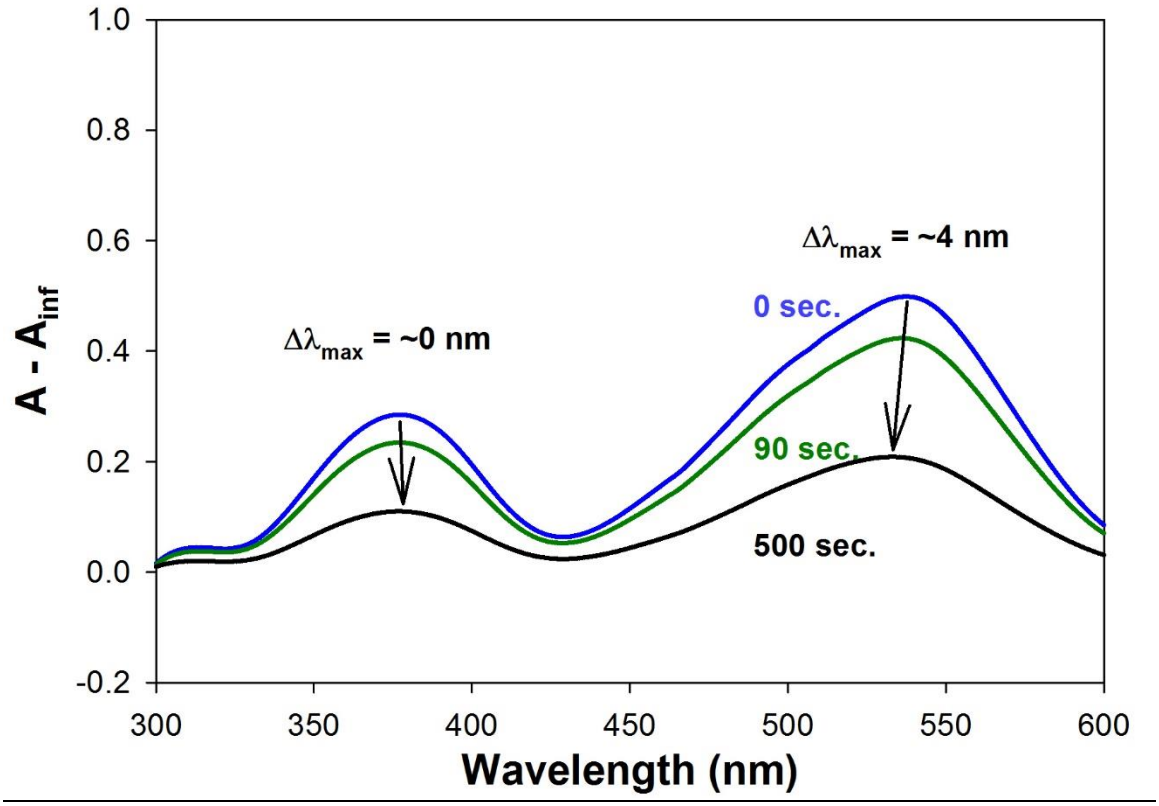

Figure A8 UV PSS spectra (0 sec.) and thermal MC to SP interconversion spectra at various times with annotated wavelength maxima shifts for **SP1**

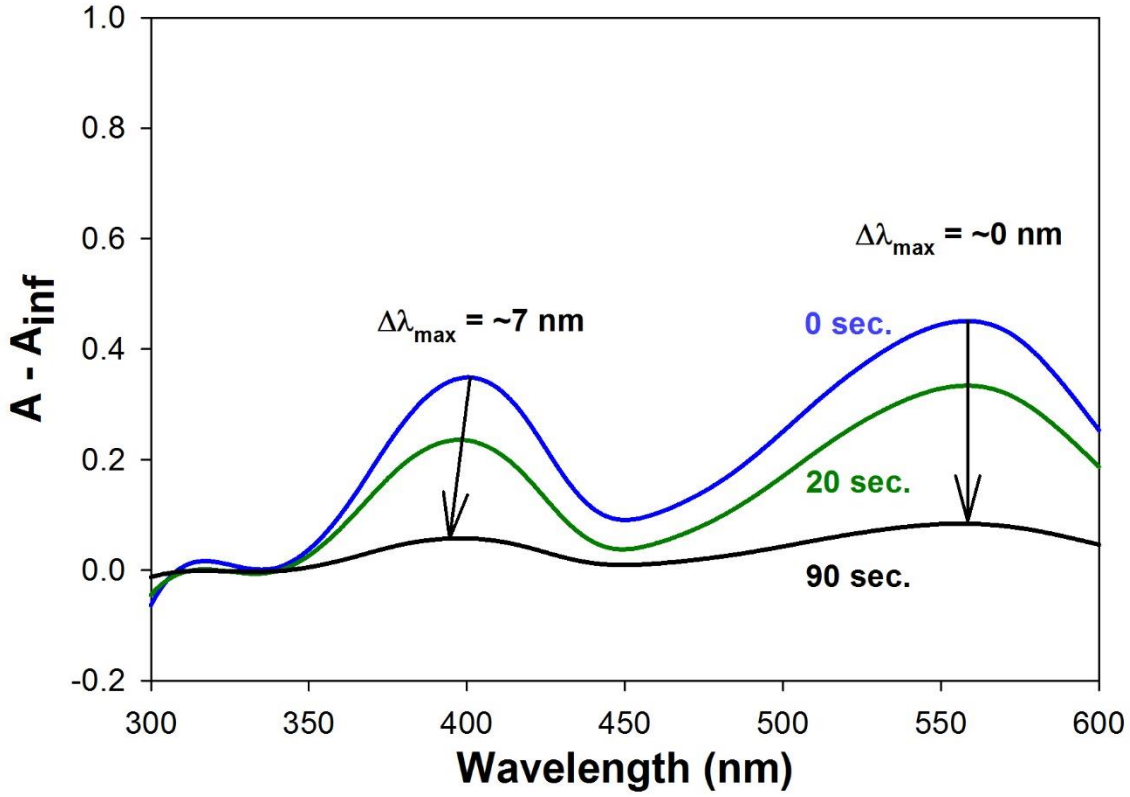

Figure A9 UV PSS spectra (0 sec.) and thermal MC to SP interconversion spectra at various times with annotated wavelength maxima shifts for **SP2**

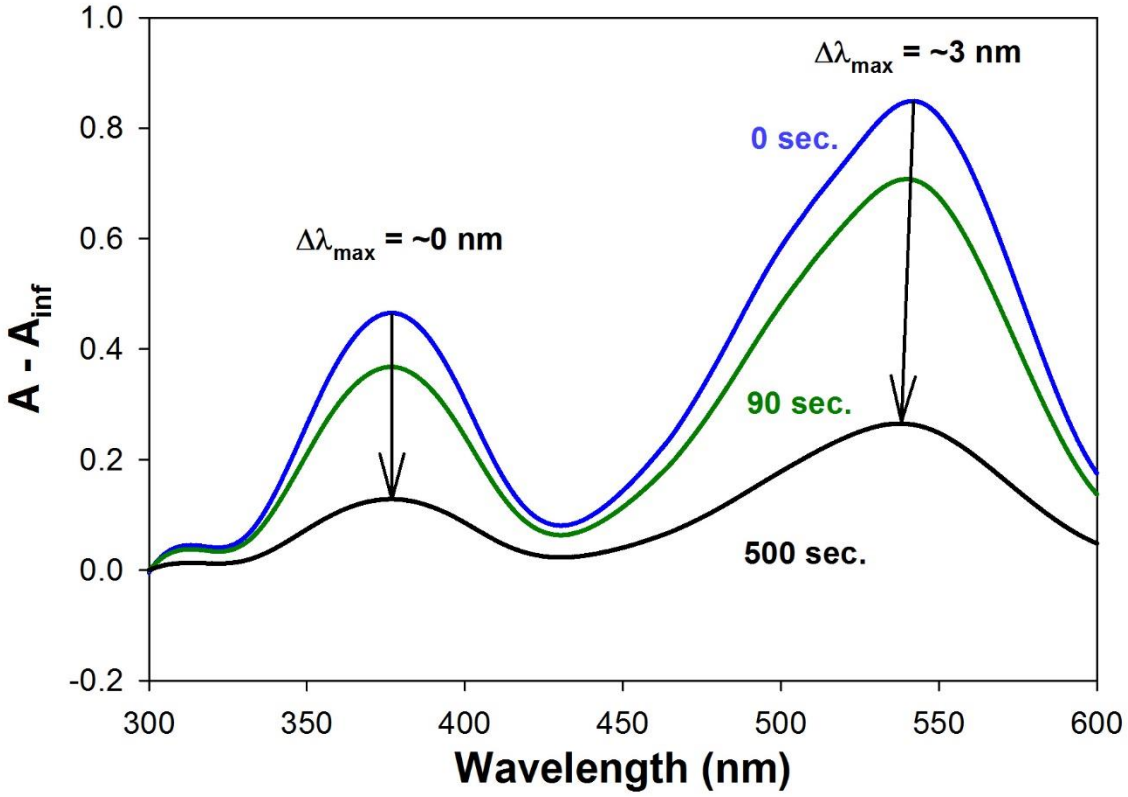

Figure A10 UV PSS spectra (0 sec.) and thermal MC to SP interconversion spectra at various times with annotated wavelength maxima shifts for **SP4**

REFERENCES

(1) Hirshberg, Y. *J. Am. Chem. Soc.* **1956**, *78*, 2304.

(2) Berman, E.; Fox, R. E.; Thomson, F. D. *J. Am. Chem. Soc.* **1959**, *81*, 5605.

(3) Wohl, C. J.; Kuciauskas, D. *J. Phys. Chem. B* **2005**, *109*, 22186.

(4) Ernsting, N. P.; Arthen-Engeland, T. *J. Phys. Chem.* **1991**, *95*, 5502.

(5) Broo, A. *Int. J. Quantum Chem.* **2000**, *77*, 455.

(6) Zhu, M.-Q.; Zhu, L.; Han, J. J.; Wu, W.; Hurst, J. K.; Li, A. D. Q. *J. Am. Chem. Soc.* **2006**, *128*, 4303.

(7) Berkovic, G.; Krongauz, V.; Weiss, V. *Chem. Rev.* **2000**, *100*, 1741.

(8) Minkin, V. I. *Russ. Chem. Rev.* **2013**, *82*, 1.

(9) Hobley, J.; Lear, M. J.; Fukumura, H. *Mol. Supramol. Photochem.* **2003**, *9*, 353.

(10) Zhang, L.-H.; Wang, Y.; Ma, F.; Liu, C.-G. *J. Organomet. Chem.* **2012**, *716*, 245.

(11) Shiraishi, Y.; Adachi, K.; Itoh, M.; Hirai, T. *Org. Lett.* **2009**, *11*, 3482.

(12) Klajn, R. *Chem. Soc. Rev.* **2014**, *43*, 148.

(13) Whelan, J.; Abdallah, D.; Wojtyk, J.; Buncel, E. *J. Mater. Chem.* **2010**, *20*, 5727.

(14) Ueda, M.; Kim, H.-B.; Ichimura, K. *Mater. Lett.* **1994**, *20*, 245.

(15) Bell, N. S.; Piech, M. *Langmuir* **2006**, *22*, 1420.

(16) Anastasiadis, S. H.; Lygeraki, M. I.; Athanassiou, A.; Farsari, M.; Pisignano, D. *J. Adhes. Sci. Technol.* **2008**, *22*, 1853.

(17) Lukyanov, B. S.; Metelitsa, A. V.; Voloshin, N. A.; Alexeenko, Y. S.; Lukyanova, M. B.; Vasilyuk, G. T.; Maskevich, S. A.; Mukhanov, E. L. *Int. J. Photoenergy* **2005**, *7*, 17.

(18) Shumburo, A.; Biewer, M. C. *Chem. Mater.* **2002**, *14*, 3745.

(19) Kong, L.; Wong, H.-L.; Tam, A. Y.-Y.; Lam, W. H.; Wu, L.; Yam, V. W.-W. *ACS Appl. Mater. Interfaces* **2014**, *6*, 1550.

(20) García, A. A.; Cherian, S.; Park, J.; Gust, D.; Jahnke, F.; Rosario, R. *J. Phys. Chem. A* **2000**, *104*, 6103.

(21) Nakahara, Y.; Yamaguchi, Y.; Iwamoto, H.; Sakamato, H.; Kimura, K. *Anal. Methods* **2012**, *4*, 4025.

(22) Scarmagnani, S.; Walsh, Z.; Lopez, F. B.; Slater, C.; Macka, M.; Paull, B.; Diamond, D. *E-J. Surf. Sci. Nanotechnol.* **2009**, *7*, 649.

(23) Sheng, Y.; Leszczynski, J.; Garcia, A. A.; Rosario, R.; Gust, D.; Springer, J. *J. Phys. Chem. B* **2004**, *108*, 16233.

(24) Minkin, V. I.; Metelitsa, A. V.; Dorogan, I. V.; Lukyanov, B. S.; Besugliy, S. O.; Micheau, J.-C. *J. Phys. Chem. A* **2005**, *109*, 9605.

(25) Wojtyk, J. T. C.; Kazmaier, P. M.; Buncel, E. *Chem. Mater.* **2001**, *13*, 2547.

(26) Keum, S.-R.; Lee, K. B.; Klazmaier, P. M.; Manderville, R.; Buncel, E. *Magn. Reson. Chem.* **1992**, *30*, 1128.

(27) Keum, S.-R.; Hur, M.-S.; Kazmaier, P. M.; Buncel, E. *Can. J. Chem.* **1991**, *69*, 1940.

(28) Becke, A. D. *J. Chem. Phys.* **1993**, *98*, 5648.

(29) Lee, C.; Yang, W.; Parr, R. G. *Phys. Rev. B* **1988**, *37*, 785.

(30) Vosko, S. H.; Wilk, L.; Nusair, M. *Can. J. Phys.* **1980**, *58*, 1200.

(31) Stephens, P. J.; Devlin, F. J.; Chabalowski, C. F.; Frisch, M. J. *J. Phys. Chem.* **1994**, *98*, 11623.

(32) Wojtyk, J. T. C.; Wasey, A.; Xiao, N.; Kazmaier, P. M.; Hoz, S.; Yu, C. Y.; Lemieux, R. P.; Buncel, E. *J. Phys. Chem. A* **2007**, *111*, 2411.

(33) Yee, L. H.; Hanley, T.; Evans, R. A.; Davis, T. P.; Ball, G. E. *J. Org. Chem.* **2010**, *75*, 2851.

(34) Frisch, M. J.; Trucks, G. W.; Schlegel, H. B.; Scuseria, G. E.; Robb, M. A.; Cheeseman, J. R.; Scalmani, G.; Barone, V.; Mennucci, B.; Petersson, G. A.; Nakatsuji, H.; Caricato, M.; Li, X.; Hratchian, H. P.; Izmaylov, A. F.; Bloino, J.; Zheng, G.; Sonnenberg, J. L.; Hada, M.; Ehara, M.; Toyota, K.; Fukuda, R.; Hasegawa, J.; Ishida, M.; Nakajima, T.; Honda, Y.; Kitao, O.; Nakai, H.; Vreven, T.; Montgomery, Jr., J. A.; Peralta, J. E.; Ogliaro, F.; Bearpark, M.; Heyd, J. J.; Brothers, E.; Kudin, K. N.; Staroverov, V. N.; Kobayashi, R.; Normand, J.; Raghavachari, K.; Rendell, A.; Burant, J. C.; Iyengar, S. S.; Tomasi, J.; Cossi, M.; Rega, N.; Millam, N. J.; Klene, M.; Knox, J. E.; Cross, J. B.; Bakken, V.; Adamo, C.; Jaramillo, J.; Gomperts, R.; Stratmann, R. E.; Yazyev, O.; Austin, A. J.; Cammi, R.; Pomelli, C.; Ochterski, J. W.; Martin, R. L.; Morokuma, K.; Zakrzewski, V. G.; Voth, G. A.; Salvador, P.; Dannenberg, J. J.; Dapprich, S.; Daniels, A. D.; Farkas, O.; Foresman, J. B.; Ortiz, J. V.; Cioslowski, J.; Fox, D. J. *Gaussian 09, Revision A.1*; Gaussian, Inc.: Wallingford, CT, 2009.

(35) Mesleh, M. F.; Hunter, J. M.; Shvartsburg, A. A.; Schatz, G. C.; Jarrold, M. F. *J. Phys. Chem.* **1996**, *100*, 16082.

(36) Mesleh, M. F.; Hunter, J. M.; Shvartsburg, A. A.; Schatz, G. C.; Jarrold, M. F. *J. Phys. Chem. A* **1997**, *101*, 968.

(37) Barone, V.; Cossi, M. *J. Phys. Chem. A* **1998**, *102*, 1995.

(38) Cossi, M.; Rega, N.; Scalmani, G.; Barone, V. *J. Comput. Chem.* **2003**, *24*, 669.

(39) Ridley, J. E.; Zerner, M. C. *Theor. Chem. Acc.* **1973**, *32*, 111.

(40) Ridley, J. E.; Zerner, M. C. *Theor. Chem. Acc.* **1976**, *42*, 223.

(41) Bacon, A. D.; Zerner, M. C. *Theor. Chem. Acc.* **1979**, *53*, 21.

(42) Zerner, M. C.; Lowe, G. H.; Kirchner, R. F.; Mueller-Westerhoff, U. T. *J. Am. Chem. Soc.* **1980**, *102*, 589.

(43) Zerner, M. C.; Correa de Mello, P.; Hehenberger, M. *Int. J. Quantum Chem.* **1982**, *21*, 251.

(44) Anderson, W. P.; Edwards, W. D.; Zerner, M. C. *Inorg. Chem.* **1986**, *25*, 2728.

(45) Hanson, L. K.; Fajer, J.; Thompson, M. A.; Zerner, M. C. *J. Am. Chem. Soc.* **1987**, *109*, 4728.

(46) Thompson, M. A.; Zerner, M. C. *J. Am. Chem. Soc.* **1991**, *113*, 8210.

(47) Zerner, M. C. In *ZINDO 9*; VCH Publishing: New York, 1991; Vol. 2, pp. 313–366.

(48) Bauernschmitt, R.; Ahlrichs, R. *Chem. Phys. Lett.* **1996**, *256*, 454.

(49) Casida, M. E.; Jamorski, C.; Casida, K. C.; Salahub, D. R. *J. Chem. Phys.* **1998**, *108*, 4439.

(50) Stratmann, R. E.; Scuseria, G. E.; Frisch, M. J. *J. Chem. Phys.* **1998**, *109*, 8218.

(51) Van Caillie, C.; Amos, R. D. *Chem. Phys. Lett.* **1999**, *308*, 249.

(52) Van Caillie, C.; Amos, R. D. *Chem. Phys. Lett.* **2000**, *317*, 159.

(53) Furche, F.; Alrichs, R. *J. Chem. Phys.* **2002**, *117*, 7433.

(54) Scalmani, G.; Frisch, M. J.; Mennucci, B.; Tomasi, J.; Cammi, R.; Barone, V. *J. Chem. Phys.* **2006**, *124*, 1.

(55) Savitzky, A.; Golay, M. J. E. *Anal. Chem.* **1964**, *36*, 1627.

(56) Steinier, J.; Termonia, Y.; Deltour, J. *Anal. Chem.* **1972**, *44*, 1906.

(57) Madden, H. H. *Anal. Chem.* **1978**, *50*, 1383.

(58) Leach, R. A.; Carter, C. A.; Harris, J. M. *Anal. Chem.* **1984**, *56*, 2304.

(59) Baedecker, P. A. *Anal. Chem.* **1985**, *57*, 1477.

(60) Gorry, P. A. *Anal. Chem.* **1990**, *62*, 570.

(61) Kim, H.; Kim, H. I.; Johnson, P. V.; Beegle, L. W.; Beauchamp, J. L.; Goddard, W. A.; Kanik, I. *Anal. Chem.* **2008**, *80*, 1928.

(62) Modica, A. P. *J. Phys. Chem.* **1968**, *72*, 4594.

(63) Eilmes, A. *J. Phys. Chem. A* **2013**, *117*, 2629.

(64) Gorner, H. *Phys. Chem. Chem. Phys.* **2001**, *3*, 416.

(65) Sciaini, G.; Wetzler, D. E.; Alvarez, J.; Fernández-Prini, R.; Laura Japas, M. *J. Photochem. Photobiol. Chem.* **2002**, *153*, 25.

(66) Haynes, W. M. *CRC Handbook of Chemistry and Physics*; 94th ed.; Taylor and Francis, 2013.

(67) Malatesta, V.; Neri, C.; Wis, M. L.; Montanari, L.; Millini, R. *J. Am. Chem. Soc.* **1997**, *119*, 3451.

(68) Aubard, J.; Maurel, F.; Buntinx, G.; Guglielmetti, R.; Levi, G. *Mol. Cryst. Liq. Cryst.* **2000**, *345*, 215.

(69) Pepe, G.; Siri, D.; Samat, A.; Pottier, E.; Guglielmetti, R. *Mol. Cryst. Liq. Cryst. Sci. Technol. Sect. Mol. Cryst. Liq. Cryst.* **1994**, *246*, 247.

(70) Minkin, V. I. *Chem. Rev.* **2004**, *104*, 2751.

(71) Bahr, J. L.; Kodis, G.; de la Garza, L.; Lin, S.; Moore, A. L.; Moore, T. A.; Gust, D. *J. Am. Chem. Soc.* **2001**, *123*, 7124.

(72) Delbaere, S.; Vermeersch, G. *J. Photchemistry Photobiol. C* **2008**, *9*, 61.

(73) Dalbaere, S.; Micheau, J. C.; Berthet, J.; Vermeersch, G. *Int. J. Photoenergy* **2004**, *6*, 151.

(74) Berthet, J.; Delbaere, S.; Carvalho, L. M.; Vermeersch, G.; Coelho, P. J. *Tetrahedron Lett.* **2006**, *47*, 4903.

(75) Hobley, J.; Malatesta, V.; Millini, R.; Montanari, L.; Parker, W. O. *Phys. Chem. Chem. Phys.* **1999**, *1*, 3259.

(76) Hobley, J.; Malatesta, V.; Giroldini, W.; Stringo, W. *Phys. Chem. Chem. Phys.* **2000**, *2*, 53.

(77) Futami, Y.; Lim, M.; Chin, L. S.; Kudoh, S.; Takayanagi, M.; Nakata, M. *Chem. Phys. Lett.* **2003**, *370*, 460.

(78) Zhang, J. Z.; Schwartz, B. J.; King, J. C.; Harris, C. B. *J. Am. Chem. Soc.* **1992**, *114*, 10921.

(79) Antipin, S. A.; Petrukhin, A. N.; Gostev, F. E.; Marevtsev, V. S.; Titov, A. A.; Barachevsky, V. A.; Strokach, Y. P.; Sarkisov, O. M. *Chem. Phys. Lett.* **2000**, *331*, 378.

(80) Holm, A.-K.; Rini, M.; Nibbering, E. T. J.; Fidder, H. *Chem. Phys. Lett.* **2003**, *376*, 214.

(81) Ganesan, R.; Remacle, F. *Theor. Chem. Acc.* **2012**, *131*, 167.

(82) Poisson, L.; Raffael, K. D.; Soep, B.; Mestdagh, J.-M.; Buntinx, G. *J. Am. Chem. Soc.* **2006**, *128*, 3169.

(83) Bernstein, S. L.; Dupuis, N. F.; Lazo, N. D.; Wyttenbach, T.; Condron, M. M.; Bitan, G.; Teplow, D. B.; Shea, J. E.; Ruotolo, B. T.; Robinson, C. V.; Bowers, M. T. *Nat. Chem.* **2009**, 326.

(84) Breukera, K.; McClafferty, F. W. *Proc. Natl. Acad. Sci. USA* **2008**, *105*, 18145.

(85) Pierson, N. A.; Chen, L.; Russell, D. H.; Clemmer, D. E. *J. Am. Chem. Soc.* **2013**, *135*, 3186.

(86) Balasubramanian, G.; Schulte, J.; Müller-Plathe, F.; Böhm, M. C. *Chem. Phys. Lett.* **2012**, *554*, 60.